

GEO Newsletter



Group for Earth Observation

No 85 - March 2025



Wildfires burning in Los Angeles are visible in this January, 9 2025 satellite image.
Credit: European Union, Copernicus Sentinel-3 imagery

GEO MANAGEMENT TEAM

General Information

John Tellick,
email:

GEO Newsletter Editor

Les Hamilton,
email: lesw.hamilton@gmail.com

Technical Consultant (Hardware)

David Simmons
email:

Webmaster and Website Matters

Vacancy
e-mail:

Management Team

David Anderson
Rob Denton
Nigel Evans: nigel.m0nde@gmail.com
Clive Finnis
Carol Finnis
Peter Green
David Simmons
David Taylor: david-taylor@blueyonder.co.uk

Useful User Groups

Weather Satellite Reports

This group provided weekly reports, updates and news on the operational aspects of weather satellites.

<https://groups.io/g/weather-satellite-reports>

SatSignal

This end-user self help group is for users of David Taylor's Satellite Software Tools, including the orbit predictor WXtrack, the file decoders GeoSatSignal and SatSignal, the HRPT Reader program, the remapper GroundMap, and the manager programs - MSG Data Manager, GOES-ABI Manager, AVHRR Manager etc.

<https://groups.io/g/SatSignal>

MSG-1

This forum provides a dedicated area for sharing information about hardware and software for receiving and processing EUMETCast data.

<https://groups.io/g/MSG-1>

GEO-Subscribers

This is the official group is for subscribers of the Group for Earth Observation (GEO), aimed at enthusiasts wishing to exchange information relating to either GEO or Earth Observation satellites.

<https://groups.io/g/GEO-Subscribers/>

Copy for the Newsletter

The Editor is always delighted to receive material for inclusion in the GEO Quarterly Newsletter. This can relate to any aspect of Earth Imaging, especially

- Technical articles concerning relevant hardware and software
- Construction projects
- Weather satellite images
- Reports on weather phenomena
- Descriptions of readers' satellite imaging stations
- Activities from overseas readers
- Letters to the Editor
- Problems and Queries for our experts to answer

Contributions should of course be original and be submitted to the editor by e-mail not later than the middle of the month preceding publication.

If your article submission contains embedded images and diagrams, please note that you must also submit copies of the original images as separate attachments: these are essential for page make-up purposes.

Materials for publication should be sent to the editor, Les Hamilton, at

wsats@leshamilton.co.uk

GEO Quarterly Back-issue Archive

GEO Quarterly has been in continuous publication since 2004, and all previous issues are available on-line as PDF copies from:

<https://leshamilton.co.uk/GEO/archive.htm>



There is also a searchable index to all titles from previous years, and this can be downloaded from:

<https://leshamilton.co.uk/soft/geoindex-setup.exe>

From the Editor

Les Hamilton

wsats@leshamilton.co.uk

The cover image, from ESA's Sentinel-3 satellite, shows the spectacular smoke plumes that emanated from the January wildfires in California. These have been covered in detail by the World's media, but you can read a brief roundup on page 8.

With data from Meteosat-12 now in full flow, Richard Osborne has been investigating the output from the new Lightning Imager instrument and details his work in a comprehensive 7-page article starting on page 9.

With the transition towards green energy considered to be essential for Earth's survival as we know it, we carry a fascinating feature on page 25 describing Europe's largest Photovoltaic Plant, which recently went on-line in Germany.

There are also articles on new types of Earth observing satellites: NISAR, developed jointly by NASA and India, which will map the planet in detail using Synthetic Aperture Radar, and the European Space Agency's *EarthCare* satellite which uses artificial intelligence to map clouds in 3D.

All the above plus numerous short features to entertain you.

Contents

AI-Powered Satellite Data Reveals Clouds in 3D	European Space Agency	4
Jebel Uweinat - a Saharan Landmark	Les Hamilton	6
Wildfires Devastate Los Angeles, California		8
Lightning – A Geostationary Perspective	Richard Osborne	9
Saturated Northern Australia	NASA Earth Observatory	16
Record Drought in Sicily	Copernicus Image of the Day	17
How New NASA, India Earth Satellite NISAR Will See Earth	NASA / JPL	18
New eruption of the Home Reef volcano, Tong	Copernicus Image of the Day	20
A green Milestone for Germany	Copernicus Image of the Day	20
Uplift in Finland's Kvarken Archipelago	NASA Earth Observatory	21
Cloud Wakes behind the Juan Fernández Islands	MODIS Web Image of the Day	23
Witznitz Solar Park -Europe's largest Photovoltaic Plant	Les Hamilton	25
Scotland's Coldest Night	Les Hamilton	27
Another Puff from Whakaari	NASA Earth Observatory	28
Satellites Reveal a Greener Antarctic Peninsula	NASA Earth Observatory	29
A23a Nears South Georgia Island	Copernicus Image of the Day	32
Jakobshavn Glacier, Greenland	European Space Agency	33
Bloom off of Australia	MODIS Web Image of the day	34
Satellites Spot a 'Ghost' Island	NASA Earth Observatory	36
Southern States Frozen Over	NASA Earth Observatory	38
Sado Island's Riches	NASA Earth Observatory	39
Ice on Lake Erie	MODIS Web Image of the Day	40
Snowfall in the Alps in Line with Historical Averages	Copernicus Image of the Day	41
Seismic Swarm in the Cyclades Islands, Greece	Copernicus Image of the Day	42
Tropical Cyclone Zelia	MODIS Web Image of the Day	43
Etna Eruption	Enrico Gobbetti	44
Central Italy	MODIS Web Image of the Day	45
Nested Calderas of Zavaritskogo Volcano	NASA Earth Observatory	46
Satellite Status		47

AI-Powered Satellite Data Reveals Clouds in 3D

European Space Agency

Launched in May 2024, ESA's **EarthCARE satellite** is nearing the end of its commissioning phase with the release of its first data on clouds and aerosols expected early next year. In the meantime, an international team of scientists has found an innovative way of applying artificial intelligence to other satellite data to yield 3D profiles of clouds.

This is particularly news for those eagerly awaiting data from EarthCARE in their quest to advance climate science.

Clouds play a critical role in Earth's climate system by reflecting sunlight back into space. This is known as the albedo effect, and by trapping heat radiating from Earth's surface, it is part of the greenhouse effect.

For example, high, thin clouds tend to warm the atmosphere because a high proportion of energy from the Sun can pass through, and they are also efficient at trapping heat radiating from Earth's surface. Low, thick clouds on the other hand, tend to have a cooling effect, as they reflect a high proportion of the incoming sunlight back out to space.

While scientists know that clouds play an extremely important role in both cooling and warming our atmosphere, there remains uncertainty when it comes to accounting for the exact influence they have on Earth's energy balance.

Moreover, given the ongoing climate crisis, there is an urgent need to understand whether changes to clouds will exert an overall cooling or warming effect in the future. Global, real time 3D cloud data would help reduce these uncertainties, improving climate predictions and helping decision-making.

Over the last decades, NASA's *CloudSat* mission has provided valuable vertical cloud profiles but was limited by infrequent revisits. Geostationary missions, such as Europe's *Meteosat Second Generation (MSG)*, on the other hand, take images over Europe every 15 minutes, but only obtain a 'top-down' view, without directly probing cloud profiles (Figure 1).

Using advanced machine learning techniques, an international team of scientists, coordinated by *ESA F-lab* and *FDL Europe*, has developed advanced machine learning techniques to create a method for generating '3D cloud profiles everywhere, all at once'.

In their proof-of-concept study, they analysed a year's worth of archived *CloudSat* and *MSG* data from 2010. The resulting paper, which was presented this week at the *Neural Information Processing Systems* conference in Canada, demonstrates how artificial intelligence can extract new insights from existing satellite observations.

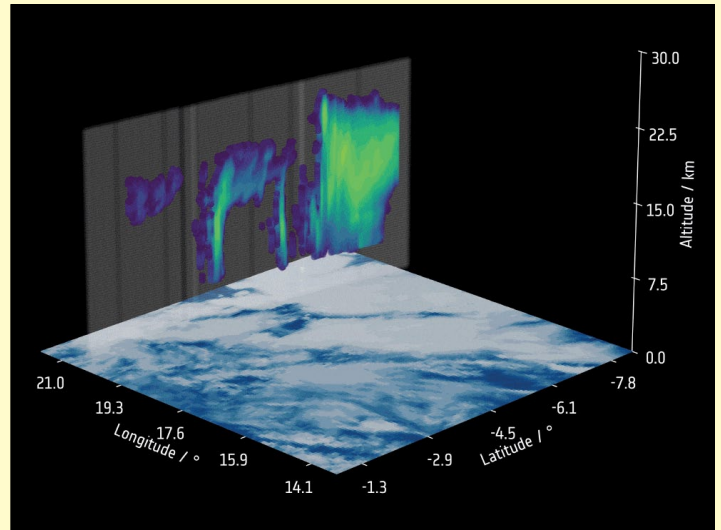


Figure 1 - Training AI to generate clouds in 3D
(An animation of this process can be viewed on the original ESA web page at the URL at the foot of this page)

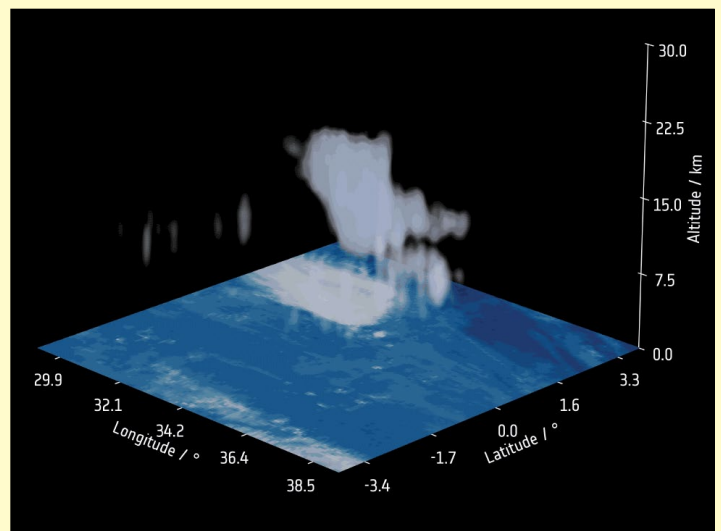


Figure 2 - Generating 3D cloud map pillars

Anna Jungbluth from ESA's Climate and Long-Term Action Division, explained,

'We carefully aligned the measured CloudSat profiles with images from MSG. This helped us understand how the 'view from top' and the corresponding cloud profiles were related.'

"We then trained machine learning models to understand this mapping and derive cloud profiles from the 2D imagery. This allowed us to extend the CloudSat profiles in both space and time."

The integration of cutting-edge AI techniques and Earth observation expertise exemplifies how innovative approaches can enhance the value of existing and future satellite missions.

https://www.esa.int/Applications/Observing_the_Earth/Space_for_our_climate/AI-powered_satellite_data_reveals_clouds_in_3D

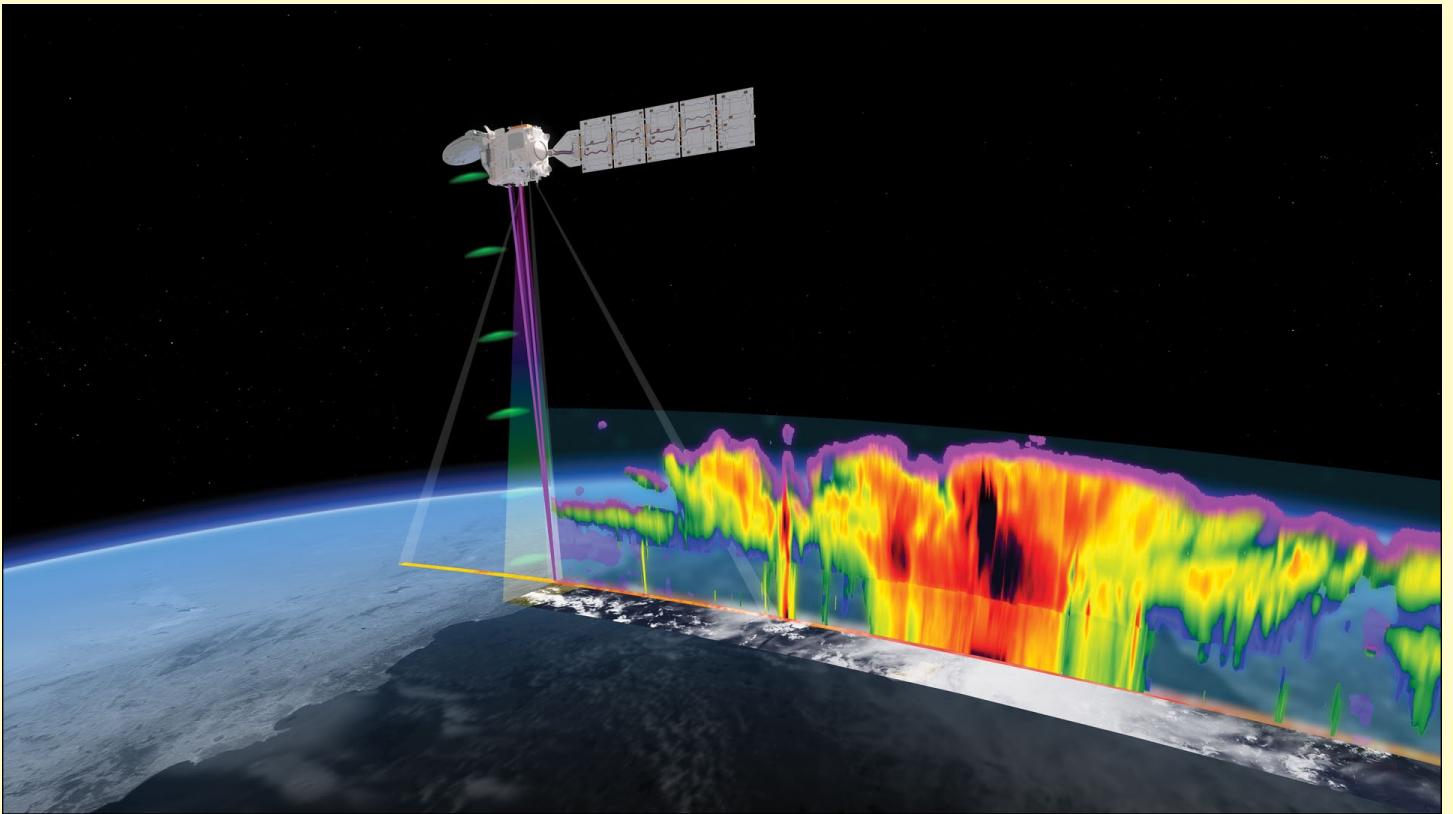


Figure 3 - EarthCARE for a better understanding of Earth's radiation balance pillars
Credit: ESA/ATG Medialab

The first animation in the body of this article (Figure 1) shows how AI was used on an MSG image (infrared channel) with a co-aligned CloudSat track. The model learns from the limited overlap of the MSG image and CloudSat track, and is able to extend the vertical cloud profile in space.

The second animation (figure 2) shows how, after the model is trained, predictions can be made for MSG images without corresponding CloudSat tracks, and 3D cloud maps can be created across space and time.

Michael Eisinger, from the *EarthCARE* project team and also from ESA's *Climate and Long-Term Action Division*, added,

“EarthCARE has already given us some very promising preliminary data and we are expecting great science from this new satellite mission. Our work generating these 3D cloud profiles lays the foundation for exploiting EarthCARE from a different angle (figure 3).”

“These new AI methods promise to maximise EarthCARE’s scientific potential and integrate its data into comprehensive global models that will push the boundaries of climate science.”

Stay tuned for more updates as EarthCARE data is harnessed to refine and expand this pioneering approach.

Note: This research has been enabled by *FDL Europe Earth Systems Lab* a public–private partnership between ESA, Trillium Technologies, the University of Oxford and leaders in commercial AI and supported by Google Cloud, Scan AI and NVIDIA Corporation.

Animations

The animations referred to above obviously cannot be reproduced here, but can be viewed in the original article: URL below.

EarthCARE for a better understanding of Earth’s radiation balance

ESA’s EarthCARE mission carries a suite of instruments to answer some critical scientific questions related to the role that clouds and aerosols play in reflecting incident solar radiation back out to space and trapping infrared radiation emitted from Earth’s surface.

Although clouds play an extremely important role in atmospheric heating and cooling, they remain one of the biggest mysteries—in fact the least understood factor—in our understanding of how the atmosphere drives the climate system.

The EarthCARE satellite’s unique set of four instruments provides a holistic view of the interplay between clouds, aerosols and radiation.

Its cloud profiling radar provides information on the vertical structure and internal dynamics of clouds, its atmospheric lidar provides cloud-top information and profiles of thin clouds and aerosols, its multispectral imager provides a wide-scene overview in multiple wavelengths, and its broadband radiometer measures reflected solar radiation and outgoing infrared radiation.

The fact that these different measurements are all taken at the same time allows scientists to better understand Earth’s radiation balance.

Jebel Uweinat - a Saharan Landmark

Les Hamilton

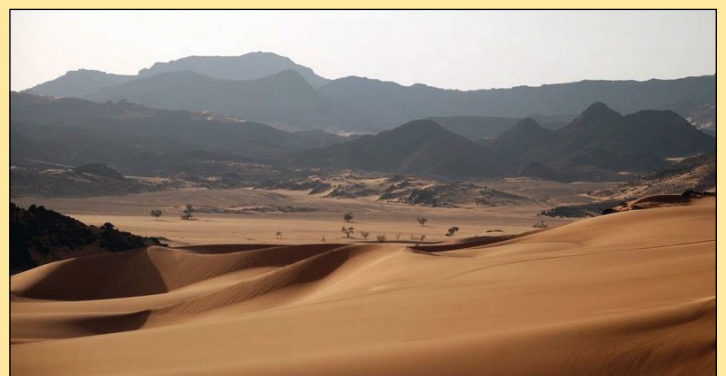


*Jebel Uweinat imaged from orbit
Credit: European Union, Copernicus Sentinel-2 imagery*

Jebel Uweinat—Arabic for ‘Mountain of the Springs’—is a rugged mountain complex in the Sahara Desert stretching almost 40 kilometres from west to east and situated in Libya, just west of its triple border with Egypt and Sudan. It is characterised by dramatic, rugged peaks and striking geologic features.

The western part of the massif consists of an intrusive, ring-shaped granite pluton approximately 25 kilometres across and includes the region’s highest summit, Mount Uwaynat, which rises to 1934 metres above sea level. To the west, this region terminates in three wadis (valleys): Karkur Hamid, Karkur Idriss and Karkur Ibrahim which drain westwards.

On its east, the granite drops as a 600 metre escarpment towards the lower eastern part which consists of Paleozoic sandstone, siltstone and shale resting upon metamorphosed Precambrian basement rocks. This region stretches as far as Karkur Talh (the Valley of Acacias), a large wadi which lies partly



A view from the east towards the rugged western part of the Jebel Uweinat massif

Image: University of Valencia Department of Education and Culture, published under Creative Commons BY 3.0 license

in neighbouring Sudan, where there is a permanent oasis called Ain El Brins.

Nowadays, water is scarce at Jebel Uweinat, as this part of the Sahara Desert receives only a few millimetres of precipitation per year, although the mountains do receive slightly more rain than the



A typical wadi in Jabel Uweinat



Petroglyphs beneath an ancient shelter



Petroglyph featuring animals and humans



Petroglyph featuring neolithic oxen at Kurkur-Talh

surrounding sand seas, and produce ephemeral streams that give the valley its name. Fewer than a hundred species of plants have been recorded here, and some of the peaks exhibit hardly any plant life at all. Such plants that do manage to eke out an existence are generally confined to temporary streams and the wadis formed from rainwater runoff. At Karkur Tahl, despite annual rainfall frequently being no greater than 10 millimetres, the region still supports acacias, grasses and other vegetation, and a scarce and elusive fauna that includes the Barbary Sheep and the Dorcas Gazelle.

Jebel Uweinat also holds clues to human habitation during past ages when the landscape was flowing with water, and is notable for its prehistoric petroglyphs. Indeed, the area is renowned for its neolithic rock art, which provides valuable insights into early Saharan cultures. Engraved in the sandstone can be seen thousands of petroglyphs representing lions, giraffes, ostriches, gazelles, oxen and human figures. Kurkur Talh contains an enormous quantity of such engravings and rock paintings, in the oldest of which, dating back to 8000 BCE, hunting scenes predominate. But the most abundant come from the more recent Neolithic period during a period when Gebel Uweinat was a much wetter and less hostile environment. Gebel Uweinat is believed to have existed in its present day arid state since around 3000 BCE,



A 7000 year old engraving of an ostrich at Kurkur-Talh

References

Jebel Uweinat
<https://earthobservatory.nasa.gov/images/80599/jebel-uweinat>

Jebel Uweinat
<https://www.jpl.nasa.gov/images/pia16679-jebel-uweinat/>

De Gebel Uweinat al altiplano
<https://conec.uv.es/mundo/iv-de-gebel-uweinat-al-altiplano-de-abu-ras/>

All above images: University of Valencia Department of Education, Research, Culture and Sports, published under Creative Commons BY 3.0 license

Wildfires Devastate Los Angeles, California

The Sentinel-3 image on the front cover of this issue illustrates the spectacular smoke plumes created by the California wildfires that broke out in early January 2025.

Between January 7 and 31, a series of destructive wildfires affected the Los Angeles metropolitan area and San Diego County in California, United States. The fires were exacerbated by drought conditions, low humidity, a buildup of vegetation from the previous winter, and hurricane-force Santa Ana winds. As the jet stream crossed mountain ranges in Southern California from north to south, mountain waves developed, accelerating wind speeds as air descended into the Los Angeles Basin and other nearby lowlands. In some places these winds attained 130 kilometres per hour in populated regions of the Los Angeles and Ventura counties but increased to as much as 160 kilometres per hour at higher elevations.

As of January 31, the wildfires had resulted in at least 29 fatalities, forced more than 200,000 to evacuate and destroyed more than 18,000 homes and structures.

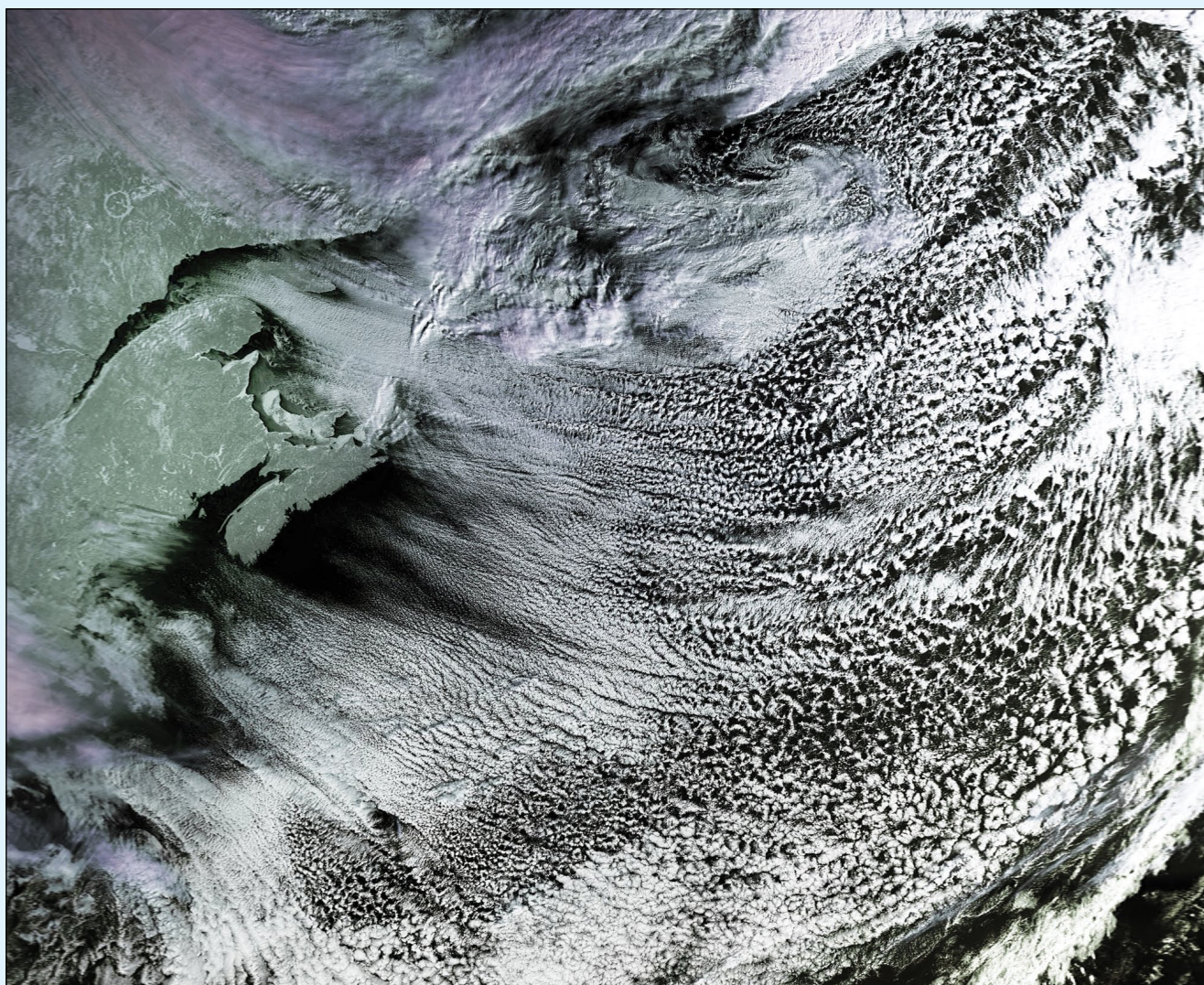
At least 230 square kilometres of land in total were destroyed by the fires.

Most of the damage came from the two largest fires: the Eaton Fire in Altadena and the Palisades Fire in Pacific Palisades, both of which had been fully contained by January 31.

Municipal fire departments and the *California Department of Forestry and Fire Protection* (CAL FIRE) fought the property fires and wildfires, which were extinguished by tactical aircraft alongside ground fire fighting teams. The deaths and damage to property from these two fires made them most likely the second and third-most destructive fires in California's history, respectively.

Open data provided by the Copernicus Sentinel satellites is essential to monitoring and mapping the extent and effects of wildfires around the world, informing damage assessments and supporting management operations.

Content credit: Wikipedia and ESA



This Metop-3 image acquired by Robert Moore on February 15, 2015 shows detail of an interesting swarm of cloud streets off the coast of Nova Scotia, Canada. The outline of the Lake Manicouagan reservoir is visible as a circular feature at upper left.

Lightning – A Geostationary Perspective

Richard Osborne

Introduction

Lightning – nature’s own fireworks display, feared by mortals and the weapon of the gods. Nevertheless, it plays an important part in the Earth’s ecological system in a number of ways including the starting of fires and generation of nitrogen oxides and ozone, all of which can play a rôle in air quality and the global climate. Until recently over Europe, Africa and the Middle East, the only method of continuous lightning monitoring has been provided by ground based radio detection systems. However, the new Meteosat Third Generation (MTG) geostationary weather satellite provides a new dimension, with the addition of an optical Lightning Imager (LI) instrument which provides day and night detection of lightning activity.

Beyond MTG, this article also considers the Geostationary Lightning Mapper (GLM) which is carried aboard the current GOES-R satellites stationed over the Americas and which can be regarded as the precursor to the MTG Lightning Imager.

Note that this article concentrates on the reception and visual display of the data provided by the LI for the interested non-professional. It is not intended to address the interpretation or application of the lightning data except at the highest possible level. Although I have tried to be accurate in this article, I am not an expert on the LI and lightning in general so I may inadvertently provide incorrect information.

MTG Data Dissemination

The MTG lightning data is disseminated on the High Volume Service Transponder 2 of *EUMETCast Europe* on channel E2H-MTG-LI. The lightning dataset consists of six different file types which are processed at Level 2 and are provided as netCDF files. However, only five types are disseminated over *EUMETCast* because of data bandwidth constraints; the remaining file type may only be accessed via the EUMETSAT Data Store.

The different file types are identified by a three letter code embedded in the (extremely long) file name.

- LEF Filtered Lightning Events (not disseminated over *EUMETCast*)
- LGR Lightning Groups
- LFL Lightning Flashes
- AF Accumulated Flashes
- AFA Accumulated Flash Area
- AFR Accumulated Flash Radiance

The first three file types (LEF, LGR, LFL) are referred to as ‘Initial Products’ and represent baseline products derived directly from the imager data. The latter three file types are referred to as ‘Accumulated Products’ and are derived from a combination of Initial Products and present the data in



a different way to aid interpretation. The detail of each file type will be described later in the article.

Within the file types, the words ‘event’, ‘group’ and ‘flash’ have very specific meanings in the context of the LI dataset and knowledge of these is essential to understanding its content. The key to this understanding requires a certain knowledge of the LI instrument itself.

MTG Lightning Imager

The Lightning Imager instrument consists of four identical high speed cameras. Each one has an optical detector with a 1170 × 1000 pixel array that takes 1000 frames (images) per second or one frame every millisecond. The basic camera arrangement is shown in Figure 1.

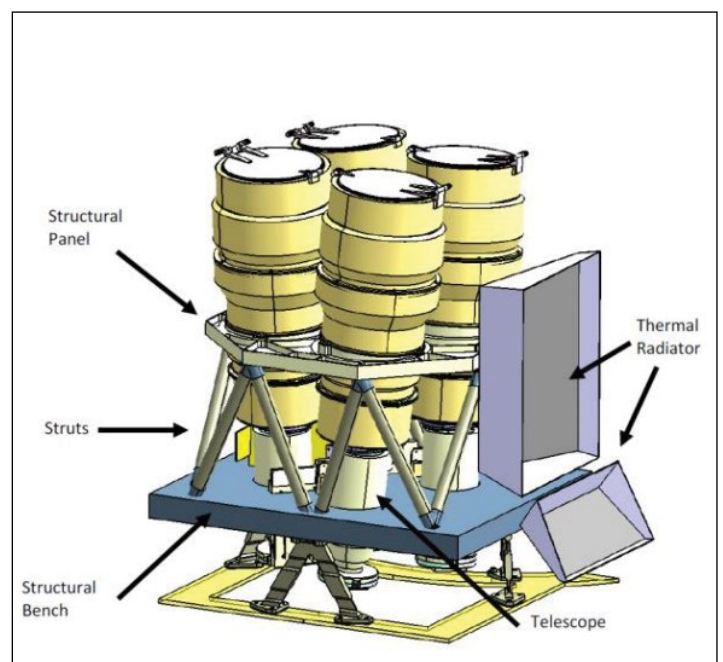


Figure 1 - General Physical Arrangement of LI Cameras

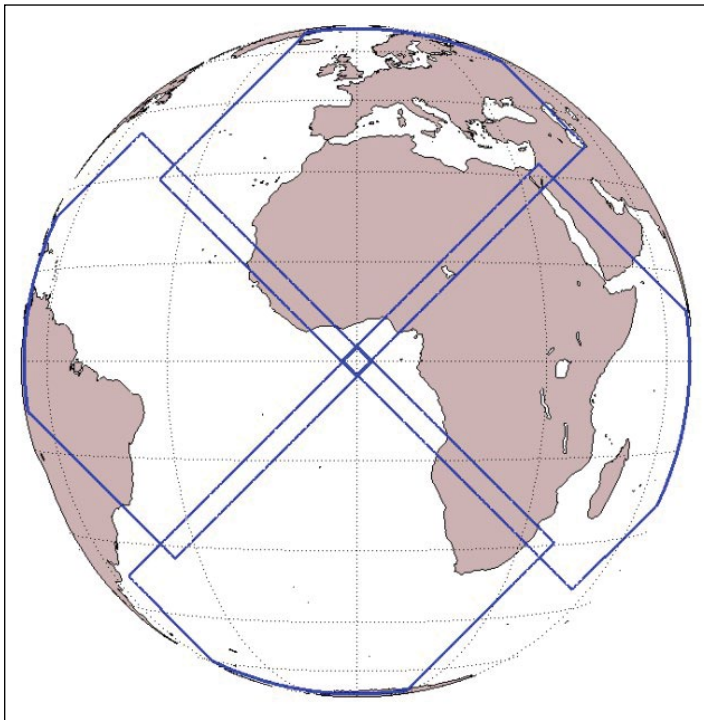


Figure 2 - The MTG LI Field of View showing the individual areas of the four cameras.

Each camera views one quadrant of the Earth with a small overlap between them, and they are imaginatively named as north, south, east and west. The coverage or Field of View (FOV) of each camera is depicted in Figure 2

At the sub-satellite point, which lies within the intersection between all four camera FOVs, a single pixel covers an area of approximately 4.5 kilometre square. Away from the sub-satellite point, the coverage area increases because of oblique viewing angles, degrading to the equivalent of 7 km square over the UK and 10 km square over Iceland.

The cameras do not see a lightning discharge directly but capture the emitted light which is scattered by obscuring clouds as a pool of light against a darker background. An example image of this effect is shown in Figure 3. Not surprisingly, the detection is better at night than day. From this image, it can be seen that the individual pools of light may be captured by only a single pixel—or multiple pixels if larger—and this observation is central to the processing of the data received from the cameras.

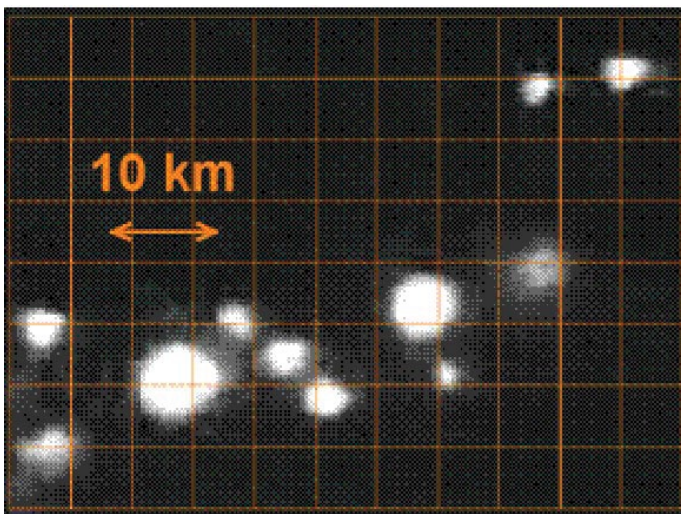


Figure 3 - Lightning Flashes viewed as pools of light from space.

The reason for the high frame rate is that a lightning flash can consist of anywhere between a single stroke and multiple strokes lasting for several seconds in total. Each stroke is detected as a transient optical pulse by the LI detector and lasts less than a millisecond when observed through clouds from above after multiple scattering. There are then periods of darkness between each stroke or groups of strokes. This is illustrated in the graph in Figure 4 which shows a flash lasting just over 400 milliseconds with multiple strokes.

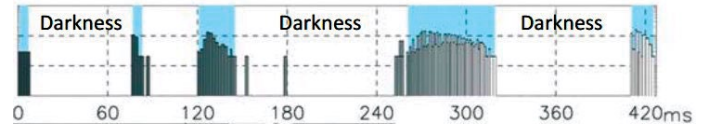


Figure 4 - Anatomy of a single flash lasting 420 milliseconds

MTG LI Product Descriptions

Every millisecond, a single optical frame/image is captured by detectors in the four cameras and this requires processing through various levels to extract the lightning detail from the background image and to determine if, for each pixel, a genuine lightning discharge has been detected with a good degree of confidence. Level 0 processing captures the raw data and passes it to Level 1 which generates a data product Level 1b. This contains all potential lightning detections, but also status flags to distinguish between true and false detections and other quality control flags. This data is then passed to Level 2 which generates the six file types (products) identified previously using a sequence of algorithms.

Initial Products

Filtered Lightning Events

The first stage in the process is to identify an event which occurs when the magnitude of a transient optical pulse, as measured by a single pixel in a camera detector, exceeds the background threshold. A filtering process then takes place at Level 1 so that by the time the data reaches Level 2, an event is deemed to be a true lightning artefact and not a false trigger. For clarity, an event is a single triggered pixel in a single camera frame (image),

When ten seconds worth of events have been processed (10,000 frames) the results are combined to produce an LEF file type which contains all the events in four separate lists, one for each camera detector. For each individual event, the list contains the key variables of timestamp, latitude and longitude, detector pixel coordinate and optical intensity (radiance). A typical file can contain several million events, and as a result they are large and not disseminated over *EUMETCast* because of constraints on data bandwidth.

Lightning Groups

A lightning stroke will often illuminate more than one pixel in a single time frame, resulting in two or more adjacent events within the same frame. When multiple events are adjacent to each other (a side or corner of the events touching), they will be placed in a single group. The formal definition of a group is one or more simultaneous events (i.e., events that occur in the same one-millisecond time

frame that register in adjacent (neighbouring or diagonal) pixels in the detector array.

A group may consist of only one event, or include many events, and is a measure of the size of the pool of light generated by a lightning stroke. Although a group may often correspond to a single lightning optical pulse, it is also possible that multiple lightning pulses occurring within the one-millisecond frame window may contribute to a group. In physical terms, the group file dataset identifies the location of lightning strokes and mirrors the information available from ground based radio lightning detection systems such as LEELA from the *Met Office*. Although the LEELA output is disseminated over *EUMETCast*, it is only available to National Meteorological Services.

Figure 5 illustrates the concept with a small portion of the detector array on the left where each square represents a pixel with coloured squares denoting a detected event. Pixels which are adjacent are then gathered into groups as shown on the right.

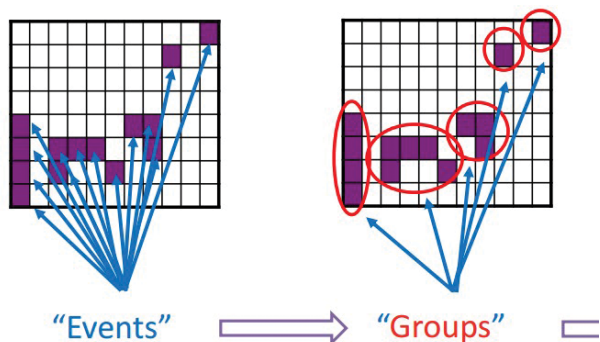


Figure 5 - The clustering of individual events into groups

When ten seconds worth of groups have been processed (10,000 frames) the results are combined to produce an LGR file type which contains details of every group within a list. For each group, the key variables include the timestamp, latitude and longitude, total radiance of the group and number of events in the group.

The geolocation of the group is described by a single latitude and longitude point which is calculated as a radiance weighted centroid to minimise the size of the file. To understand this term, first imagine the outline shape of a group represented by a flat piece of material containing all the relevant pixels. This will have a centre of mass where the material will balance perfectly on the point of a needle. Now add weights to the material for each pixel location, with the value of each weight corresponding to the radiance of that pixel. The centre of mass will shift to compensate and move towards areas of higher radiance. The final centre of mass location represents the radiance weighted centroid.

Whilst the overall size of the group can be determined by the number of associated events, the single point method of providing the location loses spatial information about the extent and shape. Pixel adjacency information is also lost.

Lightning Flashes

For the LI instrument, a flash is defined as a collection of groups sequentially separated in time by no more than 330 ms and in space by no more than 16.5 km as

determined by an algorithm. A flash may include as few as one group with a single event or it may consist of many groups, each containing many events.

To picture the process, start by selecting a group within a single frame which becomes the seed flash dataset. Examine the next 330 frames (equivalent to 330 ms) and, if a group is within the target distance, add the new group to the flash dataset, reset the frame counter and repeat. Note that there is no absolute time limit to this method. That is, as long as subsequent groups are located within the target distance and inside the 330 ms time window, they will be assigned to a single flash and the process will repeat. In practice, the duration of a flash is curtailed to around three seconds. Figure 6 extends the previous figure to show groups being clustered into a flash. Note that this only demonstrates a spatial clustering, whereas temporal clustering across multiple frames in time is also involved.

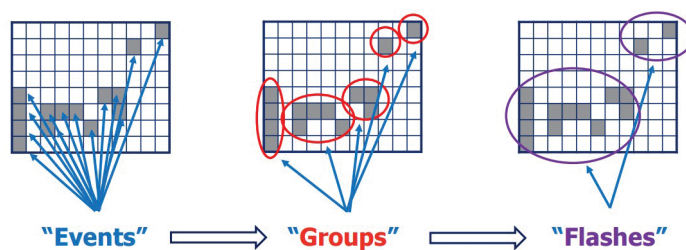


Figure 6 - Example showing the clustering of events into groups and then into a flashes.

When ten seconds worth of flashes have been processed (10,000 frames) the results are combined to produce an LFL file type which contains details of every flash within a list. For each flash, the key variables include the timestamp, latitude and longitude, total radiance of the flash, flash footprint size, flash duration and number of events/groups in the flash. As is the case for the lightning groups, the latitude and longitude of each flash is expressed as a single point using a radiance weighted centroid.

In physical terms, a flash usually encompasses multiple lightning strokes with periods of darkness in between. Note that, using the LI data alone, it is not possible to distinguish between a cloud-to-ground or cloud-to-cloud flash.

Accumulated Products

The Initial Products contain a lot of information and probably more than many users require. Also, as previously noted, the Initial Product coordinates are produced as isolated points geographically with loss of information concerning the spatial extent of groups, and flashes. The response to these observations is to present the underlying data differently to simplify the understanding of the data and restore the spatial extent information implicit in the Initial Products.

The new Accumulated Products format maps the information on to a fixed grid with 5568 rows and 5568 columns to produce a gridded product. The grid dimensions are the same as that used by the MTG FCI Optical Imager for Infra-Red images and have a nominal

2 km resolution at the sub-satellite point. Each individual product file represents 30 seconds of accumulated data. The information in each file is greatly simplified and contains only three variables in a list form: the value of the specific product and associated x and y grid references. Quality information may also be present. The use of simple x and y references in association with the grid, instead of latitude and longitude, allows a lot of information to be contained within a relatively small file size.

The addition of the spatial extent to the Accumulated Products involves going back to the original Filtered Lightning Event data, and using the events as the input to the accumulation process which identifies the flashes and the events associated with each flash. Figure 7 illustrates the accumulation process, where events linked with three separate flashes are stacked to provide an accumulated product.

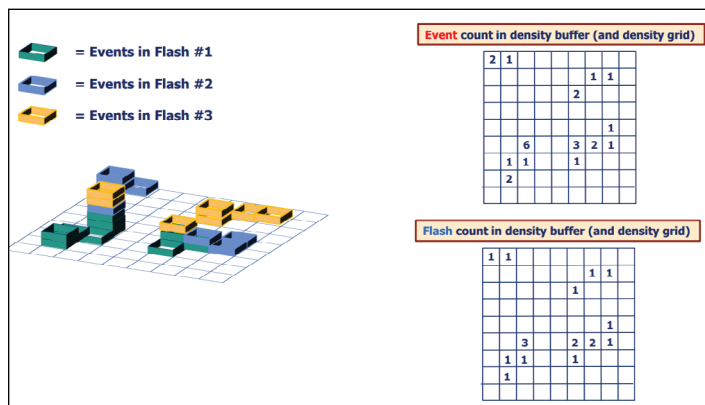


Figure 7 - Illustration of accumulation process by stacking of events associated with each flash.

This process also involves re-gridding the information from the LI detector pixel grid on to the FCI fixed 2 km grid. The process is illustrated in Figure 8, where the red squares represent individual triggered pixels (events) of the LI detector. When superimposed on the FCI 2 km grid (called pixel in the image), the grid cells marked in grey assume the state of the LI pixel. Note that the pixels on the LI detector are arranged in a diagonal pattern.

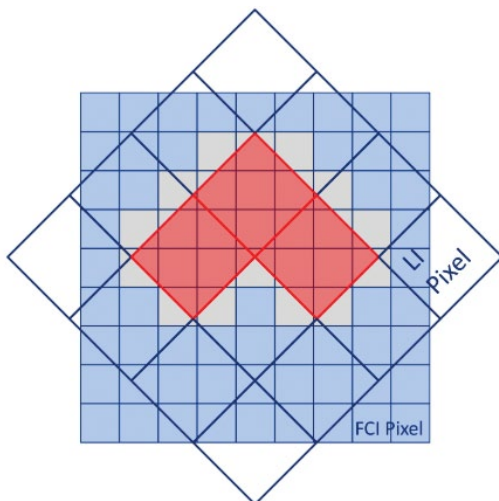


Figure 8 - LI Detector Pixel Grid (in red) superimposed on FCI grid (in blue).

A specific advantage of this method is that images produced from the Accumulated Products will line up with optical images, allowing cloud formations and lightning

activity to be correlated. Note that away from the sub satellite point, parallax errors will creep in as the optical pulses from the lightning flash seen by the satellite typically originate 10 kilometres above ground level.

Accumulated Flash Area (AFA)

The Accumulated Flash Area represents the number of contributing unique flashes associated with a single grid cell over a 30 second period. The value of the Accumulated Flash Area variable increases by one for each flash which is spatially coincident with a grid cell. Each flash could encompass multiple grid cells and therefore, the value associated with each cell represents its contribution towards a given flash. The 'area' designation arises because the value of the variable for each and every grid cell within the area (footprint) of a given flash is incremented by one.

In physical terms, this product can provide the flash rate for a grid cell which is determined by dividing the cell value by the total accumulation time.

Accumulated Flash (AF)

The Accumulated Flash provides the total number of normalised events that occur within a grid cell over a 30 second period. In other words, count the number of events that occur within a grid cell for a single flash and then divide this figure by the total number of events associated with that flash. This provides the fractional contribution of each grid cell for a given flash and is presented as a unit-less ratio.

In physical terms, this product represents the accumulated density of the lightning events within the flashes that contribute to the accumulation over a given time period. For example, a compact flash with a small area footprint will generate high values for the associated grid cells and a large area flash will generate low values. It also highlights regions of more frequent and smaller flashes.

Accumulated Flash Radiance (AFR)

Each event in a flash has a radiance value attached to it. For each flash, identify all the events that occur and sum the value of all the associated radiances within a grid cell. Repeat this exercise for as many flashes that occur within the specified 30 second period and add the results together to arrive at the final figure. Note that the value only represents the flash radiance contribution within a given grid cell and not the total radiance from each flash. The radiance values have units of power, so integrating these measurements over a period of time provides an indication of the amount of energy received by a given pixel on the LI detector. Any reference to area averaging for this product is incorrect and is subject to revision.

To summarise—for all flashes occurring within a grid cell over a given time period, the AFA provides a lightning flash rate, the AF provides an event density measurement and the AFR provides an indication of the total energy detected.

MTG LI Visualisation

As all the files are delivered in netCDF form, they can be viewed with *Panoply*. Unfortunately, because of the way

the netCDF file is constructed, *Panoply* cannot interpret the X and Y coordinates as georeferenced variables, so cannot plot the lightning data on to a basemap. However, some useful statistical information can be obtained from the data as demonstrated by the graphs in Figures 9 and 10 derived from the same 30 second timeslot. The first graph illustrates that one grid cell detected noticeably more flashes than any other and the second that one grid cell detected noticeably more energy but they are not the same cell.

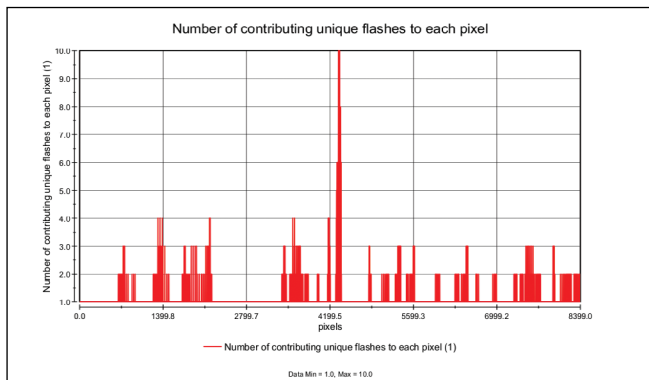


Figure 9 - Graph derived from Accumulated Flash Area file demonstrating range of observed values of flash count over 30 seconds.

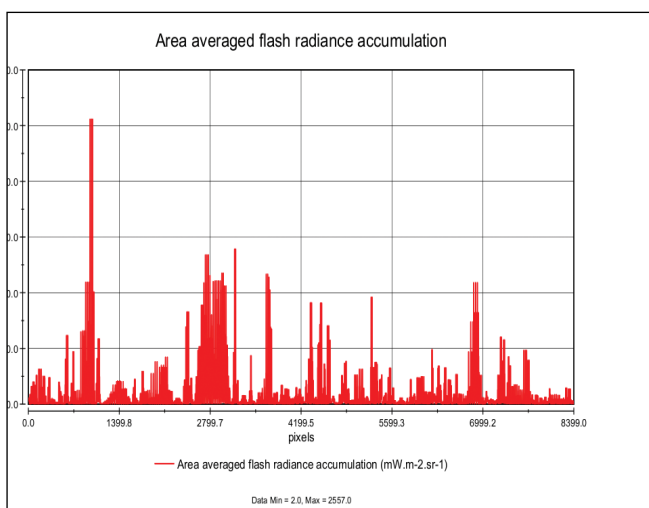


Figure 10 - Graph derived from Accumulated Flash Radiance demonstrating range of observed values of total radiance detected over 30 seconds.

Visualisation of the lightning data requires a bespoke application and I am only aware of two that are readily available and work 'Out of the Box'. I am not counting *SatPy* because this is only a *Python* package and requires a script to make it do anything.

The first is the recently introduced MTG-I application from Roman Zamiesal written in *C#* which can visualise all five LI products disseminated over *EUMETCast* and apply them as an overlay to images produced by the MTG FCI instrument. The relevant window of the application is shown in Figure 11. For LGR and LFL, I note that two different variables are visualised. One is the radiance but the other is not specified. Perhaps it is the number of events?

The second is my own application which is written in *Python*. As I prepared it as a self-contained Windows

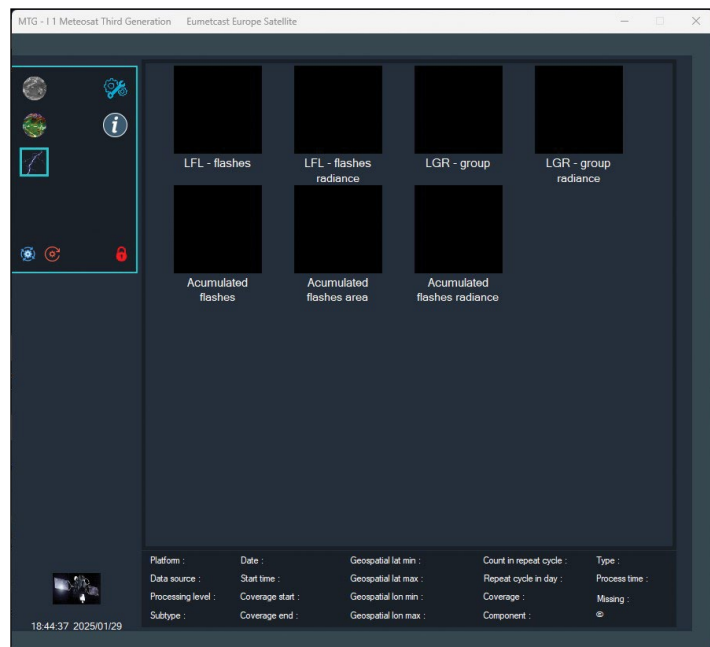


Figure 11 - Lighting display window of MTG-I application providing thumbnails of Initial and Accumulation products.

executable file driven solely by a graphical user interface (GUI) for my own ease of use, I count it as a bespoke application. The user interface is shown in Figure 12.

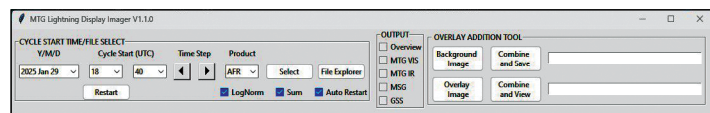


Figure 12 - The Graphical User Interface for my MTG Lightning Imaging Application.

This only caters for the accumulated files as these products appear to provide the best interpretation of the underlying data. As its input, the application imports 20 files at a time which each contain 30 seconds worth of data and stacks them to provide an output representing 10 minutes worth of accumulated data. It can generate an overview of lightning activity on a basemap or provide an image that can be applied as an overlay on a background geostationary optical image provided by a third party application. It can also combine the overlay with the background image. An example of an overview image is shown in Figure 13.

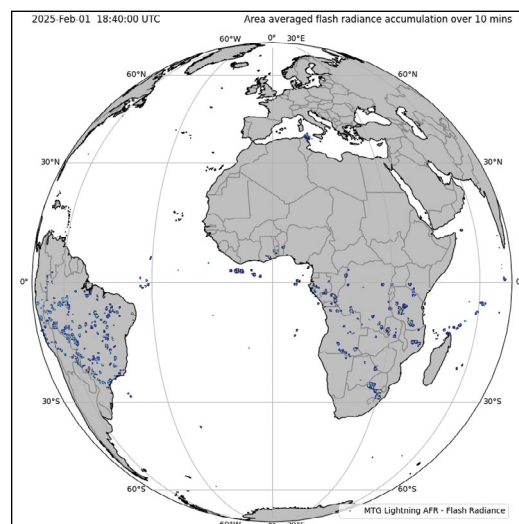


Figure 13

This is a typical overview image generated by MTG Lightning Display Imager showing radiance accumulation.

Geostationary Lightning Mapper (GLM)

As I alluded in the introduction, the MTG LI is preceded by an optical lightning detector, called the GLM, aboard the GOES-R series GOES-16 satellite which launched at the end of 2016. I have no doubt that the MTG LI draws heavily on the experience gained from the GLM. Indeed, the production method of the Initial Products appears to be almost identical to those developed for the GLM. I will now describe the operation of the GLM using the same categories as those of the MTG LI.

GLM Data Dissemination

The GLM lightning data is disseminated on the High Volume Service Transponder 1 of *EUMETCast Europe* on channel E1H-TPG-1 for GOES East and E1H-TPG-4 for GOES West. These are the same channels as the GOES ABI Imager data but specific permission for the GLM data in these channels is required from *EUMETSAT Ops* via the *EOportal*.

The lightning dataset consists of only one file type, and each disseminated file contains 15 Level 2 files in netCDF format, each containing 20 seconds of data, within a compressed TAR archive making a total of 5 minutes worth. The Level 2 files are exactly the same as those available from internet sources and contain many features of the MTG Initial Data. *EUMETCast* does not disseminate any other GLM file type.

GLM Lightning Imager

The Lightning Imager instrument consists of a single high speed camera. It has an optical detector with a 1372×1300 pixel array that takes 500 frames (images) per second, or one frame every 2 milliseconds. The coverage or Field of View (FOV) of each camera is depicted in Figure 14.

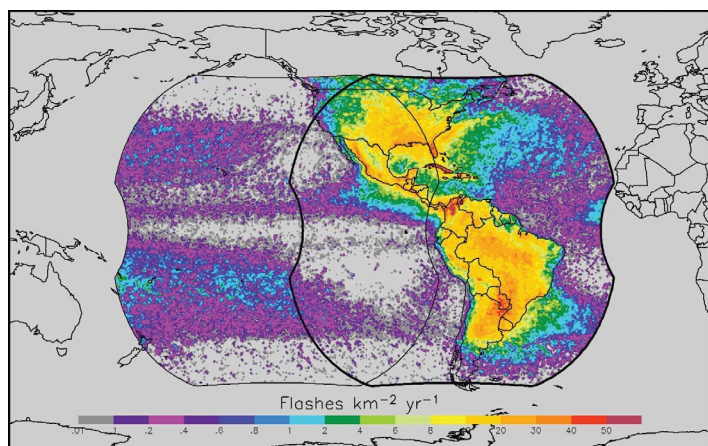


Figure 14 - The Field of View for GLM on GOES West (Light outline) and GOES East (Heavy Outline)

At the sub-satellite point, a single pixel covers an area of approximately 8 km square. Away from the sub-satellite point, the coverage area increases because of oblique viewing angles, degrading to the equivalent of 14 km square at the edge of the FOV.

GLM Product Descriptions

Every 2 milliseconds, a single optical frame is captured, and this requires processing through various levels to

extract the lightning detail from the background image and to determine if, for each pixel, a genuine lightning discharge has been detected with a good degree of confidence. An excellent quick guide to GLM lightning products may be found at:

https://www.star.nesdis.noaa.gov/goes/documents/GLM_Quick_Guides_May_2019.pdf

Level 2 Product

There is only one file type at Level 2 which contains event, group and flash data generated in a similar way that of the MTG LI instrument. One major difference is that the radiation intensity is expressed as energy instead of radiance, which is a power measurement.

Level 3 Products

The original design for the GLM only called for the production of a Level 2 product. However, the GLM developers anticipated the future use of derived products and ensured that the Level 2 files contained, as far as possible, information for this purpose. The rationale for these products has been covered in the equivalent MTG LI section of this article. Texas Tech University was commissioned to produce a series of derived products with a staggered introduction which are now available as gridded Level 3 products.

The Level 3 products are issued on a fixed grid with 5424 rows and 5424 columns. This is the same grid structure used by the GOES-R ABI Optical Imager for Infra-Red images and has a nominal 2 km resolution at the sub-satellite point. Each Level 3 file contains one minute of gridded data.

At the time of writing, GLM Level 3 files in netCDF format are available from the *NASA Earthdata portal* which will become the one-stop shop for all NASA Earth science data by the end of 2026. Currently, this L3 dataset contains the Flash Extent Density (FED), Total Optical Energy (TOE) and Minimum Flash Area (MFA) products. Other products are proposed but their eventual distribution depends on the perceived value to forecasters.

Flash Extent Density (FED)

The Flash Extent Density was the first Level 3 gridded product to be developed. It is the number of unique flashes spatially coincident with a grid cell over a defined period which is one minute for a disseminated Level 3 file. It is equivalent to the MTG LI Accumulated Flash Area product.

Total Optical Energy (TOE)

The Total Optical Energy is the sum of all optical energy that is observed within each grid cell over a defined period. It is measured in femtojoules, which is 10^{-15} Joule. The MTG LI Accumulated Flash Radiance offers a similar measurement but in milliwatts. However, relative values in an image will be the same locally.

Minimum Flash Area (MFA)

The Minimum Flash Area is the smallest area of any flash spatially coincident with a grid cell over a defined period. It is measured in square kilometres. There is no similar measurement by the MTG LI instrument.

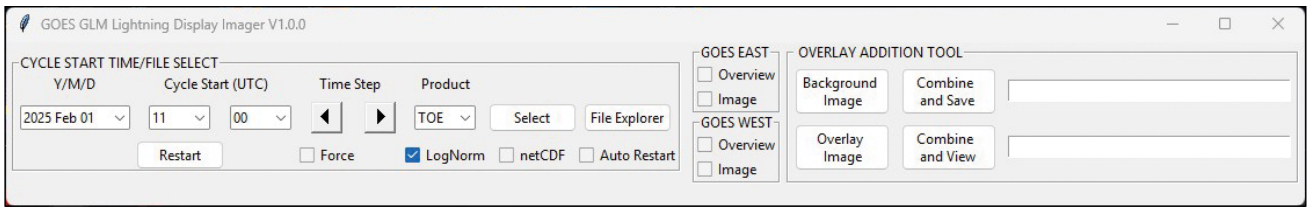


Figure 15 - The Graphical User Interface for my GLM Lightning Display Imaging Application

GLM Lightning Visualisation

As all the Level 2 files are delivered in netCDF form, they can be viewed with *Panoply*. Unfortunately, because of the way the netCDF file is constructed, *Panoply* cannot interpret the X and Y coordinates as georeferenced variables so cannot plot the lightning data on to a basemap. However, some useful statistical information can be obtained from the data as with the MTG Initial Products.

For the Level 3 files, *Panoply* is able to interpret the coordinates as georeference variables so it can plot the gridded data variables on to a base map which is useful for an initial quick look.

However, as this article and my own interests were based on only using data available over *EUMETCast*, I looked for applications (not *Python* scripts) that could visualise the GLM lightning data without recourse to the internet. I couldn't find any apart from one, but that only worked under *Linux* so it was a case of DIY.

As I had already produced a *Python* based GUI application for the MTG LI, I considered adapting this to cater for the GLM. In programming terms, an adaption for the Level 2 GLM products appeared to be relatively trivial but I really wanted to visualise Level 3 products which provide a more informative view of the lightning activity.

I managed to locate an open source *Python* package called '*glmtools*' on GitHub, which generates the Level 3 files from a Level 2 file input that had been prepared by the Texas Tech University as part of their work for NASA. Unfortunately, the package was all but incomprehensible to me as it seemed chaotic in its structure and was performing some quite scary calculations. However, with the help of an example script, I was able to (just) establish entry and exit points to the package and merge it with my existing GUI *Python* code. Finally, I was able to produce it as a single *Windows* executable file.

My GLM lightning application has the same capability as the MTG LI version and can produce an overview of lightning activity based on gridded data for GOES East and GOES West as well as images for use as an overlay. As a bonus, it can also produce Level 3 netCDF files containing one minute of data that provide the same information as those available from the *Earthdata* portal. However, as I discovered, the process requires a lot of number crunching and takes about three minutes to convert 10 minutes worth of Level 2 data into the equivalent Level 3 output on my reasonably powerful Ryzen 5500 PC, and consumes around 10 GB of RAM into the bargain!

The user interface for the GLM Lightning Display Imager is shown in Figure 15. It caters for both GOES East and GOES West (but not simultaneously) and can produce the FED, TOE and MFA products as an overview or as an image. The latter can be applied as an overlay to background ABI images produced by GOES ABI Manager or *EUMETCastView*.

An example of the overview output for GOES East is shown in Figure 16 and for GOES West is shown in Figure 17. The lightning activity for GOES West is very sparse as suggested by the annual lightning density map shown in Figure 14.

At the time of writing, the *GOES Lightning Display Imager* is still undergoing fine tuning. However, if anyone is interested in obtaining a copy, drop me a line at info@woodcroft.me.uk

If I consider that the application is suitable for public release, I will post a message on the MSG-1 Groups website <https://groups.io/g/MSG-1> with details of a download location.

Reference

Panoply - <https://www.giss.nasa.gov/tools/panoply/>

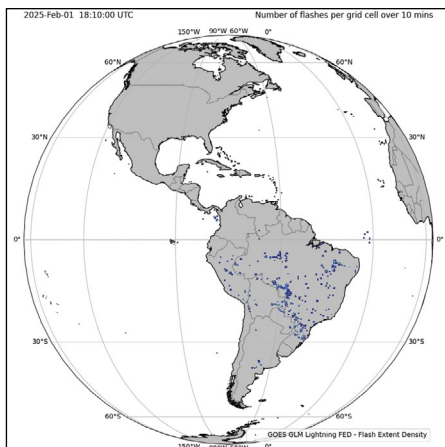


Figure 16 - Typical overview image generated by GLM Lightning Display Imager for GOES East showing Flash Extent Density.

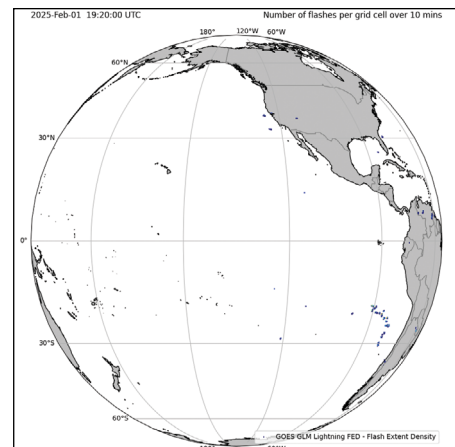


Figure 17 - Typical overview image generated by GLM Lightning Display Imager for GOES West showing Flash Extent Density.

Saturated Northern Australia

NASA Earth Observatory

Story by Lindsey Doermann



Figure 1 - Comparison of the lakes between 2002 and 2004
NASA Earth Observatory images by Lauren Dauphin, using MODIS data from NASA EOSDIS LANCE

Grasslands and cattle ranches sprawl across the hot Barkly Tableland area of Australia's Northern Territory. But when its rainy seasons are especially rainy, a network of ephemeral lakes can become inundated, with water covering thousands of square kilometres.

Two rather wet years in a row allowed Tarrabool Lake and Lake Sylvester, seen in the images above, to expand appreciably. The rainy seasons in 2022–2023 and 2023–2024, which stretch from October through April, were both amongst the top ten wettest recorded in northern Australia since 1900. The *Australian Bureau of Meteorology* reported that rainfall was 'very much above average' in this region of the Northern Territory in both seasons.

This series of images, acquired by the Moderate Resolution Imaging Spectroradiometer aboard NASA's Aqua and Terra satellites, shows the evolution of Tarrabool Lake and Lake Sylvester between November 2022 and November 2024.

Near the start of the 2002 wet season (left), only Lake Sylvester appears to contain any water. Rains later in the season, including several days of downpours in early March 2023, helped fill in the lakes enough that water persisted into the start of the next rainy season.

In November 2023 (centre), Tarrabool Lake is visible where the land was previously dry, and Lake Sylvester has expanded and merged with adjacent ephemeral lakes. The ensuing 2023–2024 wet season included the tenth wettest January and second wettest March on record for northern Australia. Contributing to that, severe tropical cyclone Megan brought widespread rainfall to the region in March 2024. The Northern Territory's Barkly Highway flooded so severely in places following that event that fish could be seen swimming across the road.

Early in the 2024–2025 wet season, the lakes covered more area than at similar times in the past two years. The OLI (Operational Land Imager) on the Landsat 8 satellite captured figure 2 (overleaf) showing their extent on October 30, 2024. Lake Sylvester had merged with nearby Corella Lake and Lake Deburgh. Likewise, the water in Tarrabool Lake had connected with an area known as Eva Downs Swamp to the northwest forming a single freshwater wetland. Both systems are considered important areas for waterbirds. Together, when fully flooded, the wetlands span approximately 4,750 square kilometres, nearly the size of the state of Delaware.

According to a report from the *Australian Bureau of Meteorology* and the *Commonwealth Scientific and Industrial Research Organisation* (CSIRO), the



Figure 2 - The lakes as imaged by Landsat 8 on October 30, 2024
 NASA Earth Observatory image by Lauren Dauphin, using Landsat data from the U.S. Geological Survey.

amount of annual rainfall in the Barkly region has trended upward in recent decades, and evaporation rates have declined. Still, rainfall is highly variable

from year to year. It falls more reliably from December to March, when monsoonal weather patterns tend to form.

Record Drought in Sicily

Copernicus Image of the Day



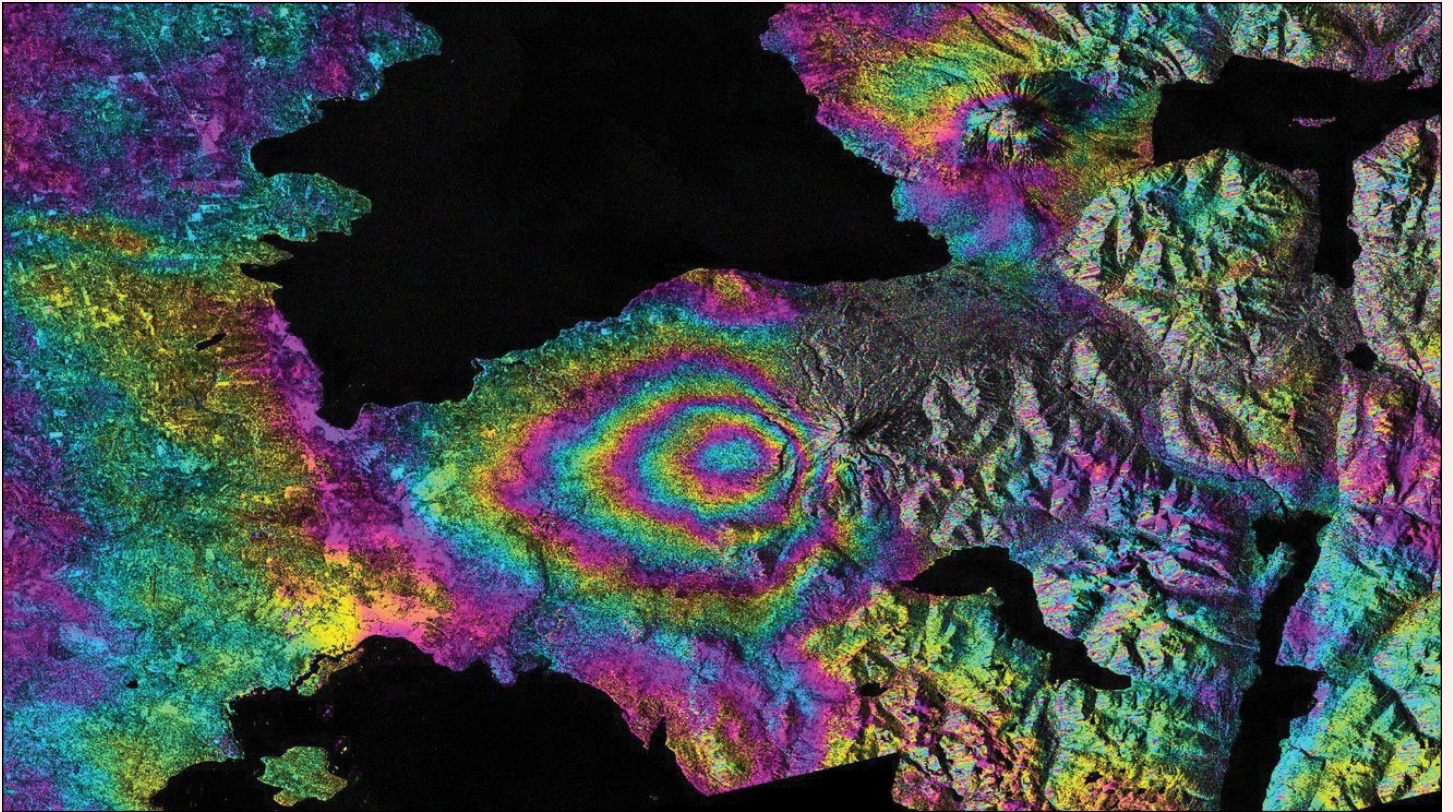
Credit: European Union, Copernicus Sentinel-2 imagery

In 2024, Sicily, Italy faced its worst drought in almost 20 years, with nearly empty reservoirs and water rationing affecting up to two million people. In response, authorities declared a state of emergency, with plans to manage the drought through the reintroduction of desalination plants.

Lake Caccamo, located in Sicily, is shown in this Copernicus Sentinel-2 image acquired on 25 July 2024. The lake used to be one of the largest in Sicily, but on 1 August, reached only 18 million cubic metres in comparison to its capacity of 100 million cubic metres.

How new NASA, India Earth Satellite NISAR will see the Earth

Nasa JPL



NASA's Jet Propulsion Laboratory used radar data taken by ESA's Sentinel-1A satellite before and after the 2015 eruption of the Calbuco volcano in Chile to create this interferogram showing land deformation. The colour bands west of the volcano indicate land sinking. NISAR will produce similar images.

Credit: ESA/NASA/JPL-Caltech

Set to launch within a few months, NISAR will use a technique called synthetic aperture radar to produce incredibly detailed maps of surface change on our planet.

When NASA and the Indian Space Research Organization's (ISRO) new Earth satellite NISAR (NASA-ISRO Synthetic Aperture Radar) launches in coming months, it will capture images of Earth's surface so detailed they will show how much small plots of land and ice are moving, down to fractions of a centimetre. Imaging nearly all of Earth's solid surfaces twice every 12 days, it will see the flex of Earth's crust before and after natural disasters such as earthquakes: it will monitor the motion of glaciers and ice sheets, and it will track ecosystem changes, including forest growth and deforestation.

The mission's extraordinary capabilities come from the technique noted in its name: synthetic aperture radar, or SAR. Pioneered by NASA for use in space, SAR combines multiple measurements, taken as a radar flies overhead, to sharpen the scene below. It works like conventional radar, which uses microwaves to detect distant surfaces and objects, but steps up the data processing to reveal properties and characteristics at high resolution.

To get such detail without SAR, radar satellites would need antennas too enormous to launch, much less operate. At 12 meters wide when deployed, NISAR's radar antenna reflector is as wide as a city bus is long. Yet it would have to be 19 kilometres in diameter for the mission's L-band instrument, using traditional radar techniques, to image pixels of Earth down to 10 metres across.

Synthetic aperture radar '*allows us to refine things very accurately,*' said Charles Elachi, who led NASA space borne SAR missions before serving as director of NASA's Jet Propulsion Laboratory in Southern California from 2001 to 2016. '*The NISAR mission will open a whole new realm to learn about our planet as a dynamic system.*'

How SAR Works

Elachi arrived at JPL in 1971 after graduating from Caltech, joining a group of engineers developing a radar to study Venus' surface. Then, as now, radar's allure was simple: It could collect measurements day and night and see through clouds.

The team's work led to the Magellan mission to Venus in 1989 and several NASA space shuttle radar missions. An orbiting radar operates on the same

principles as one tracking planes at an airport. The space borne antenna emits microwave pulses toward Earth. When the pulses hit something, a volcanic cone, for example, they scatter. The antenna receives those signals that echo back to the instrument, which measures their strength, change in frequency, how long they took to return and if they bounced off of multiple surfaces, such as buildings.

This information can help detect the presence of an object or surface, its distance away, and its speed, but the resolution is too low to generate a clear picture. First conceived at Goodyear Aircraft Corporation in 1952, SAR addresses that issue.

'It's a technique to create high-resolution images from a low-resolution system,' said Paul Rosen, NISAR's project scientist at JPL.

As the radar travels, its antenna continuously transmits microwaves and receives echoes from the surface. Because the instrument is moving relative to Earth, there are slight changes in frequency in the return signals. Called the Doppler shift, it's the same effect that causes a siren's pitch to rise as a fire engine approaches then fall as it departs.

Computer processing of those signals is like a camera lens redirecting and focusing light to produce a sharp photograph. With SAR, the spacecraft's path forms the 'lens,' and the processing adjusts for the Doppler shifts, allowing the echoes to be aggregated into a single, focused image.

Using SAR

One type of SAR-based visualisation is an interferogram, a composite of two images taken at separate times that reveals the differences by measuring the change in the delay of echoes. Though they may look like modern art to the untrained eye, the multicoloured concentric bands

of interferograms show how far land surfaces have moved: the closer the bands, the greater the motion. Seismologists use these visualisations to measure land deformation from earthquakes.

Another type of SAR analysis, called polarimetry, measures the vertical or horizontal orientation of return waves relative to that of transmitted signals. Waves bouncing off linear structures like buildings tend to return in the same orientation, while those bouncing off irregular features, like tree canopies, return in another orientation. By mapping the differences and the strength of the return signals, researchers

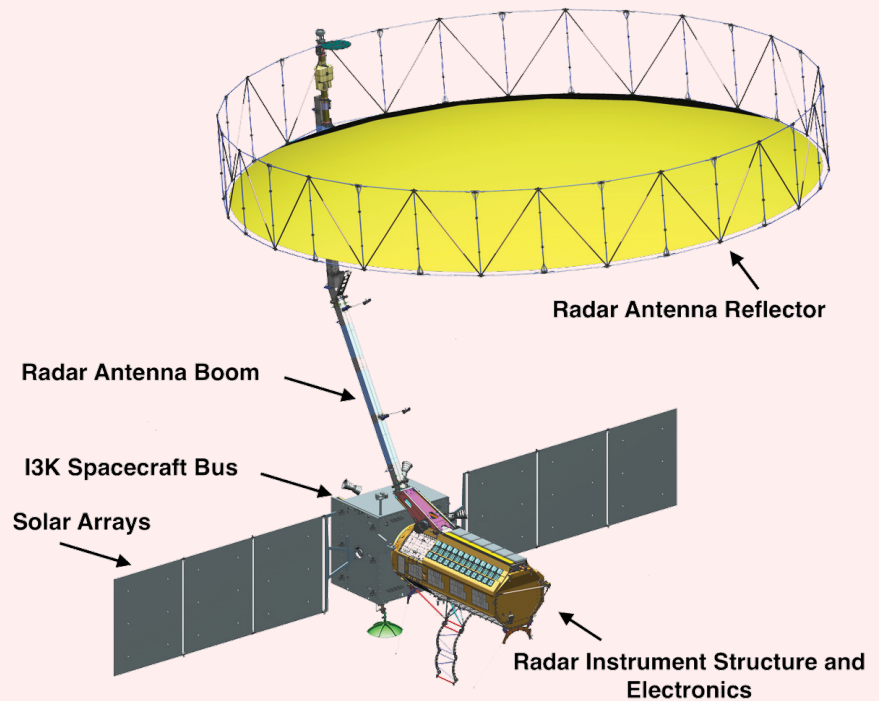
can identify an area's land cover, which is useful for studying deforestation and flooding.

Such analyses are examples of ways NISAR will help researchers better understand processes that affect billions of lives.

'This mission packs in a wide range of science toward a common goal of studying our changing planet and the impacts of natural hazards,' said Deepak Putrevu, co-lead of the ISRO science team at the Space Applications Centre in Ahmedabad, India.

Learn more about NISAR at:

<https://nisar.jpl.nasa.gov>



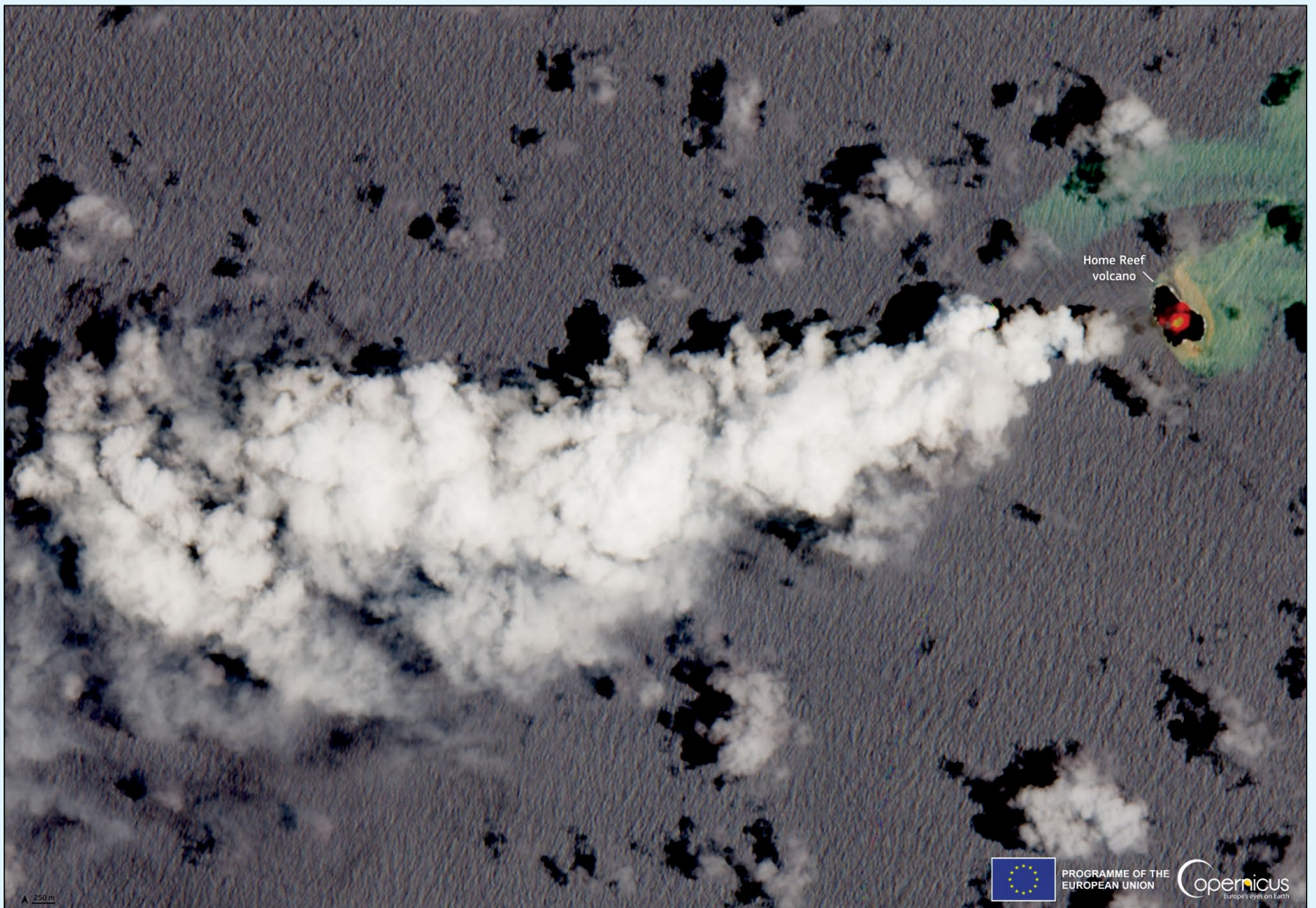
NISAR Diagram
Credit: NASA/JPL-Caltech



AN artist's concept of NISAR in orbit
Credit: NASA/JPL-Caltech

New Eruption of the Home Reef Volcano, Tonga

Copernicus Image of the Day



Credit: European Union, Copernicus Sentinel-2 imagery

Home Reef is an underwater volcano in the Tonga Archipelago, characterised by cyclical eruptions which can last from a few days to several weeks. While not constantly active, its eruptions can produce hazards such as tsunamis, ash fall, and pyroclastic flows, as in the eruption of January 2022, which caused widespread damage to nearby islands.

On 7 December 2024, a new eruption began at the Home Reef volcano in Tonga. This marks the second eruptive

period of Home Reef in 2024, following one that occurred between June and July. A strong thermal anomaly was detected by one of the Copernicus Sentinel-2 satellites on the same day that the eruption began, along with a horizontally spreading plume extending over 8 kilometres.

The Copernicus Sentinel satellites deliver key information on volcanic activity worldwide, providing insights on eruptions and their impacts to help keep affected communities safer.

A Green Milestone for Germany

In 2024, renewable energies made up 59% of Germany's total electricity generation, up from 56% 2023. For the first time, wind and solar overtook fossil fuels as energy sources, thanks in large part to renewable energy deployment policies, including more accessible wind permits and an increase in solar energy installations. German authorities report that in 2024, there was more than a 10% drop in fossil fuel energy sources. Onshore wind contributed over 25% to the country's electricity generation, while solar energy recorded the largest growth. This **Copernicus** Sentinel-2 image, acquired on October 15, 2024, shows the Nordergründe offshore wind farm in the North Sea off the coast of Germany.



Credit: EU, Copernicus Sentinel-2 imagery

Uplift in Finland's Kvarken Archipelago

NASA Earth Observatory

Story by Lindsey Doermann

Some 20,000 years ago, during the Last Glacial Maximum, the Baltic Sea lay under a sheet of ice up to 3,000 metres deep. Scientists estimate that the weight of that ice pressed the land down more than 500 metres.

Since the glaciers receded and the weight was lifted, the land has been bouncing back. The rates of uplift—known as glacial isostatic adjustment or isostatic rebound—in this region are among the highest on Earth. By one estimate, 700 hectares of new land—about twice the size of Central Park in New York City—rise from the sea each year along the margins of the Gulf of Bothnia, the Baltic Sea's northern arm.

This uplift is especially apparent in the Kvarken Archipelago of Finland. The area, seen in this image acquired by the OLI (Operational Land Imager) on Landsat 8, is an agglomeration of islands that is constantly changing as the land rises. Its approximately 5,600 islands and 2,400 kilometres of shoreline form labyrinthine waterways that present hazards to ships but exploration opportunities for canoers and kayakers. The Kvarken Archipelago, along with the High Coast region across the gulf in Sweden, is designated as a UNESCO World Heritage site.

The terrain emerging from the sea has revealed remarkable glacial formations. On and around the island of Björkö, shown in (figure 1) this detailed view, unique features known as De Geer moraines have surfaced thanks to isostatic rebound. These washboard-like ridges form when water running beneath the ice deposits boulders, stones, and finer material at the ice edge. When the ice retreats or a large block breaks away, another moraine begins to form at the new edge.



Figure 1

A Landsat-9 image acquired at sunset, of tiny islands in the Kvarken Archipelago. Open ocean extends to the horizon.

NASA Earth Observatory images by Wanmei Liang, using Landsat data from the U.S. Geological Survey



Figure 2

This detailed Landsat image shows the island of Björkö in Finland's Kvarken Archipelago. The island appears to be divided into elongated fields coloured tan and different shades of green. Glacial features called De Geer moraines are visible around the coastline as narrow parallel islands.

NASA Earth Observatory images by Wanmei Liang, using Landsat data from the U.S. Geological Survey



Figure 3

Photograph taken at sunset of tiny islands in the Kvarken Archipelago. Open ocean extends to the horizon.

Photo: Hendrik Morkel,

De Geer moraines typically measure 1 to 2 kilometres long and 2 to 5 metres tall, spaced 50 to 200 metres apart. Scientists think their presence and spacing are related to the speed of ice-margin retreat, the water depth in which they were formed, and the terrain beneath the ice. LiDAR-based digital elevation models have recently revealed the existence of more De Geer moraines in southern and western Finland than previously realised.

The constant emergence of new land after the ice's disappearance affected how people ultimately developed the area. For example, the land on which the town of Vaasa was founded was a forested island in the early 14th century. The island later merged with the mainland, and Vaasa grew throughout the 17th and 18th centuries as a thriving harbour and trading point.

Still, the land continued to rise, causing the coastline to migrate farther and farther from the town. In August 1852, a napping peddler's pipe ignited a fire that destroyed much of the settlement. Officials took the opportunity to reestablish Vaasa about six kilometres to the west to make it a coastal city once again.

Remnants of the original town are preserved in 'Old Vaasa' (or Vanha-Vaasa).

The islands, peninsulas, and coastlines around the Kvarken Archipelago and the Gulf of Bothnia will continue to morph and evolve. Since the ice retreated, the land has risen at least 286 metres; this figure corresponds to the elevation of the ancient shore and so-called 'world's highest coastline,' located across the gulf at Skuleberget in Sweden's High Coast. The remaining 100 metres or so of depression should equilibrate over the next several thousand years, scientists say.

In that time, the sea level will continue to drop relative to the land and the Gulf of Bothnia will continue to narrow. Millennia from now, the shores of Finland and Sweden may even connect at the narrowest point, rendering the northern Gulf of Bothnia an inland lake. However, the exact nature of these changes will depend on how much global sea level rise—driven by ice melt and thermal expansion of ocean water—offsets the regional land uplift. Currently, the rate of regional uplift, at about 9 millimetres per year, outpacing the current 3.4 millimetres of annual global sea level rise.

Cloud Wakes behind the Juan Fernández Islands

MODIS Web Image of the Day



Image Credit: MODIS Land Rapid Response Team, NASA GSFC

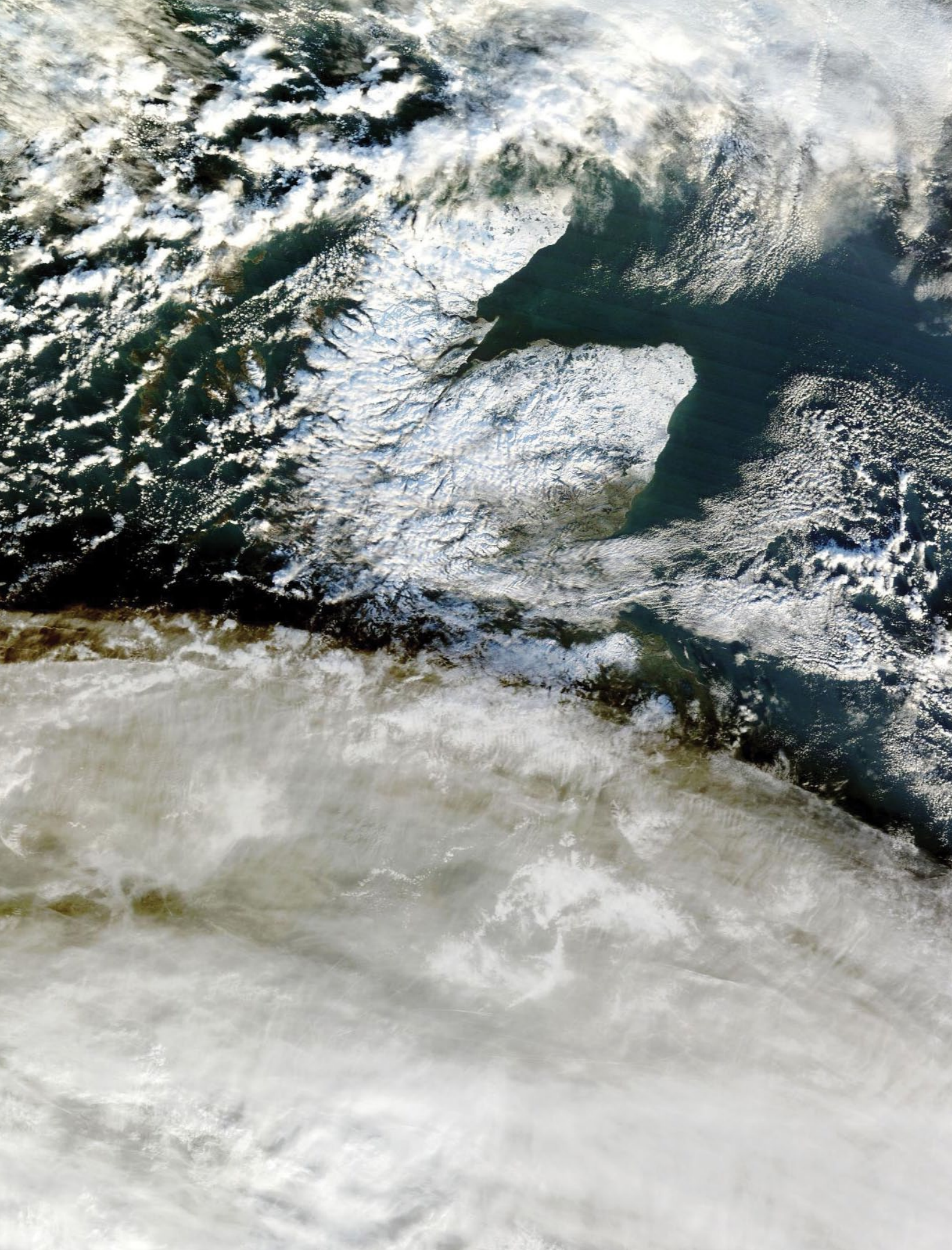
Steady wind and two tall, tiny islands combined to create stunning patterns in the clouds off the coast of Chile in late December 2024. The Moderate Resolution Imaging Spectroradiometer (MODIS) on NASA's Aqua satellite acquired this true-colour image of cloud wakes on December 25.

The dark 'V' shapes cut into the clouds look similar to wakes created as a boat speeds over water. In this case, however, the wakes are formed as the atmosphere moves around stationary objects—the peaks of two tall volcanic islands that jut up above the ocean surface. In both cases, the creation of wakes follows principles of fluid dynamics, that branch of physics that focuses on the behaviour of fluids in motion. Both liquids and gases are classified as 'fluids'.

When wind blows across a level surface and encounters a tall, immobile object (in this case, volcanic peaks), its forward motion is interrupted as it is forced to diverge around both sides of the object. This uneven motion creates turbulence in the

atmosphere and, when conditions are right, disrupts cloud formation behind the object. The shape of the clouds on the lee side of islands can take on various shapes, from complex swirling eddies to more simple shapes, such as these cloud wakes.

The Juan Fernández islands lie about 600 kilometres west of Valparaíso, Chile. There are three islands in this rugged archipelago: Robinson, Santa Clara, and Alejandro Selkirk. They rise from an east-west submarine ridge, with Isla Alejandro Selkirk and Isla Robinson Crusoe rising tall above the ocean surface. In this image, the smaller island, Isla Alejandro Selkirk, sits to the west and can be seen as green at the bottom of the dark 'V' in the clouds. Isla Robinson Crusoe, though larger, is hidden under the thick bank of marine stratocumulus clouds. Nonetheless, its location is given away by the cloud wave created behind its tallest peak. Isla Santa Clara is an islet that lies between these two islands but it doesn't rise high enough to significantly disrupt air flow or cloud formation.



Scotland is seen freezing hard and largely under snow on January 4, 2025 in this image acquired by NASA's Terra Earth observation satellite
Image: NASA Worldview Snapshots (<https://wvs.earthdata.nasa.gov>)

Witznitz Solar Park -Europe's largest Photovoltaic Plant

Les Hamilton



Witznitz Solar Park is visible in this Copernicus Sentinel-2 image acquired on 1 December 2024.
Credit: European Union, Copernicus Sentinel-2 imagery

Witznitz Solar Park, located near Leipzig, Saxony in the east of Germany, was Europe's largest photovoltaic plant when it was completed in early 2024. Built on a former brown coal open-cast mining dumping ground, the park spans approximately five square kilometres and consists of more than 1.1 million solar modules. When it started operation in April 2024 the plant was producing an estimated output of more than 650 MW. And by the time plant achieved full capacity in the summer of 2024, the park was estimated to be capable of powering around 200,000 homes and reducing annual carbon dioxide emissions by some 250,000 tonnes.

What's special about this plant is that it uses the existing grid infrastructure developed for the former lignite mining operation to feed power directly into the 50 Hertz transmission network. A transformer station was built next to the power plant to increase the output from the plant to 380 kilovolts.

Shell will purchase the solar energy from the Witznitz Energy Park at a fixed price for the next 15



Aerial view over the solar module array
Photo: MOVE ON Energy GmbH



Photovoltaic panels in harmony with Nature
 Photo: MOVE ON Energy GmbH



Photovoltaic panels in harmony with Nature
 Photo: MOVE ON Energy GmbH



The view between two Photovoltaic panel arrays
 Photo: MOVE ON Energy GmbH

years and in turn, sell it to Microsoft to operate the software giant's data centres in Saxony. This means that the plant does not require any state subsidies.

In a new approach to project planning, the developer—*MOVE ON Energy*—has made an important contribution to the re-naturalisation of 120 hectares of the former mining areas, dedicated to environmental protection, social projects, and the promotion of local tourism. In addition to electricity production, extensive nature conservation measures have been implemented to promote local biodiversity. These include the planting of almost 21 kilometres of field hedges as a visual screen and as a breeding area, the creation of flower meadows and the construction of nesting boxes for birds and bats on what was formerly an industrial wasteland.

The newly created recreational paths for hikers and cyclists make the region an attractive local recreation area.

References

Wikipedia

- https://de.wikipedia.org/wiki/Energiepark_Witznitz

Copernicus Image of the Day

- <https://www.copernicus.eu/en/media/image-day-gallery/witznitz-solar-park-europes-largest-photovoltaic-plant>

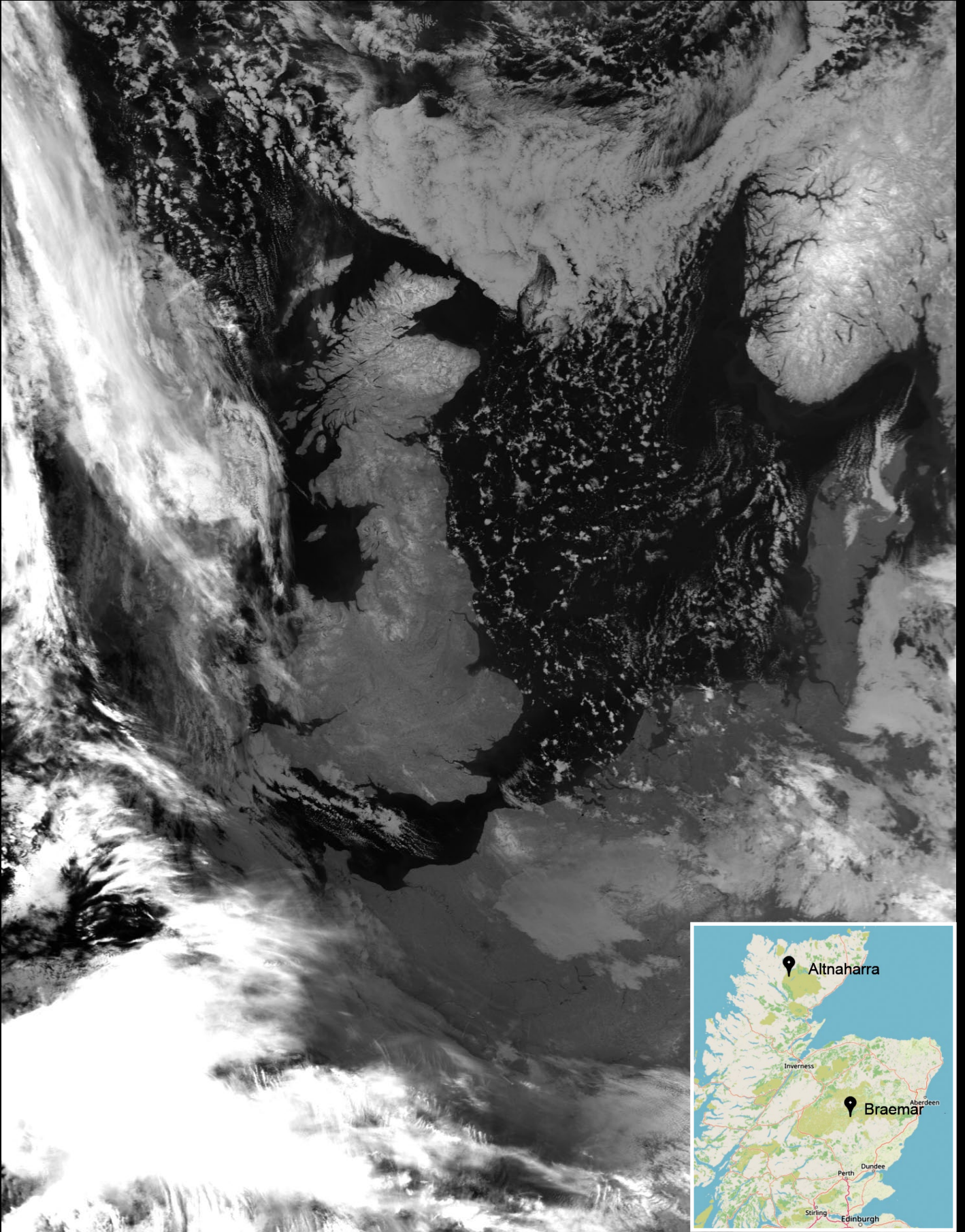
Move On nimmt riesigen Energiepark Witznitz in Betrieb

- <https://www.erneuerbareenergien.de/technologie/solar/move-nimmt-riesigen-energiepark-witznitz-betrieb>

Energiepark Witznitz

- <https://www.moveon-energy.de/energiepark-witznitz/>

Scotland's Coldest Night



Overnight on January 9-10 this year, the hamlet of Altnaharra in the far north of Scotland endured Britain's coldest night of the winter when a temperature of -18.9°C was recorded. This Metop-C image depicts Great Britain cloud free with the highlands buried in snow. This was the lowest recorded temperature for 15 years, but the all-time record of -27.2°C was recorded jointly by Braemar (February 1895 and January 1982) and Altnaharra (December 30, 1995).

Credits: Metop image - NOAA CLASS Archive Scotland Map - Openstreetmap.com

Another Puff from Whakaari

NASA Earth Observatory

Story by Adam Voiland



Ash plume rising from Whakaari/White Island on January 7, 2025

NASA Earth Observatory image by Michala Garrison, using Landsat data from the U.S. Geological Survey

The partially submerged volcano in New Zealand's Bay of Plenty is called Whakaari/White Island. It's a fitting name for the perpetually puffing and occasionally explosive stratovolcano offshore from North Island.

The volcano's name is a combination of Te Puia o Whakaari (a Maori phrase for 'dramatic volcano') and White Island, the name given to it by British explorer James Cook in 1769 after noticing that it puffed steam almost continuously.

Conditions were on the calm side when the OLI-2 (Operational Land Imager-2) on Landsat 9 captured this image of the volcano on January 7, 2025. In an update on January 13, the local hazards monitoring group *GeoNet* noted that the volcano was undergoing a period of 'heightened unrest' and had been emitting weak-to-moderate steam and gas plume emissions and 'small amounts of ash' for the previous two-to-three weeks.

Due to the ash, authorities elevated the aviation colour code to orange.

"Currently, this activity is not affecting air traffic as the dominant wind is blowing the ash away from the mainland and the plume is very low elevation—a few thousand feet," stated Craig Miller, a geophysicist at GNS Science. He added that, while this type of passive ash emission is technically an eruption, events need to be more explosive to be classified as a minor eruption (level 3 on the regional system for Volcanic Alert Levels).

GeoNet geologists think magma is quite close to the surface based on the high vent temperatures. When magma is near the surface, it becomes easier for rising gases to pull small bits of cooled magma into the plume as ash fragments. Sometimes hot gases rising through the vent also cause bits of the crater wall to flake off into the plume and become an additional source of ash.

Satellites Reveal a Greener Antarctic Peninsula

NASA Earth Observatory

Story by Lindsey Doermann

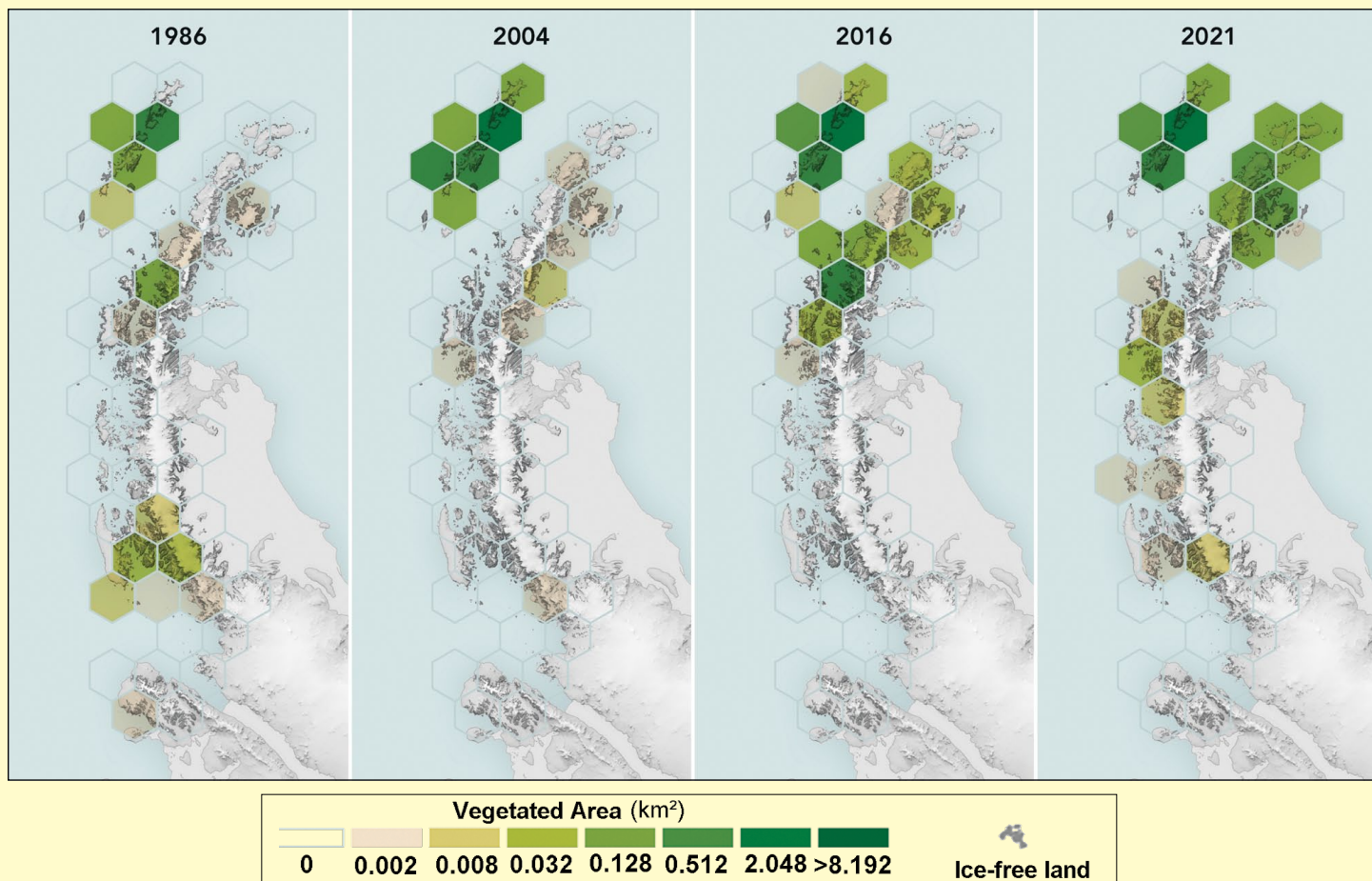


Figure 1

Maps of the Antarctic Peninsula showing the increased greening between 1986 and 2021
NASA Earth Observatory maps by Michala Garrison, based on data from Roland, T.P., et al. (2024)

The white, monochromatic vistas of Antarctica, a continent practically synonymous with ice, are becoming more verdant—at least around some of its edges. According to an analysis of 35 years of observations from Landsat satellites, the amount of vegetated land on the Antarctic Peninsula has increased more than tenfold since 1986. As glaciers shrink and temperatures warm, plant life is finding more opportunity to move into this and other cold-climate regions. The expansion of greenery on the Antarctic Peninsula may signal a shift in its ecology, say researchers, raising questions about its future.

Using observations from Landsat 5 through Landsat 8, scientists determined that the area of vegetated land on the Antarctic Peninsula grew from 0.86 to 11.95 square kilometres between 1986 and 2021. Notably, the expansion of green space accelerated starting in 2016. The research, published in *Nature Geoscience* in October 2024, was led by environmental scientist Tom Roland of the University of Exeter and remote sensing expert Olly Bartlett of the University of Hertfordshire.

Their results are encapsulated in the maps shown in figure 1. The panels show the amount of green on the peninsula's ice-free land below 300 metres elevation at select years during the study period. The shade of each hexagon corresponds with the area of land where levels of plant greenness and density, as determined by the satellite-based *Normalized Difference Vegetation Index* (NDVI), were high enough to indicate the 'almost certain' presence of vegetation. The NDVI values were derived from cloud-free Landsat observations acquired during the month of March of each year, which typically encompasses the end of the growing season. The maps show significant expansion in vegetation cover across the South Shetland Islands (at the top-left of each panel) and down the western side of the peninsula to nearly the southern limit for plant growth.

Past field studies on the Antarctic Peninsula have shown that mosses dominate its green areas, forming expansive 'carpets' and vertically accumulating 'banks', similar to those shown in the photograph of Ardley Island overleaf (figure 2).



Figure 2 - Ardley Island, which lies 150 kilometres north of the tip of the Antarctic peninsula
Photo courtesy of Dan Charman (University of Exeter).

Both build up layers of new growth each year. In earlier work, Roland and colleagues carbon-dated core samples taken from moss banks along the western side of the peninsula. They discovered that the rates at which moss was accumulating had increased in the past 50 years, indicating an uptick in biological activity amid climatic changes.

These results got scientists wondering if vegetation was not only expanding its territory upward but also outward. So Roland, Bartlett, and their team tapped into the decades-long Landsat record. 'Based on the core samples, we expected to see some greening,' Roland said, 'but I don't think we were expecting it on the scale that we reported here.'

The pace of greening was surprising, as well. 'When we first ran the numbers, we were in disbelief,' stated Bartlett. But the results, based on two different measures of greenness, kept coming out the same. 'The rate itself is quite striking, especially in the last few years.'

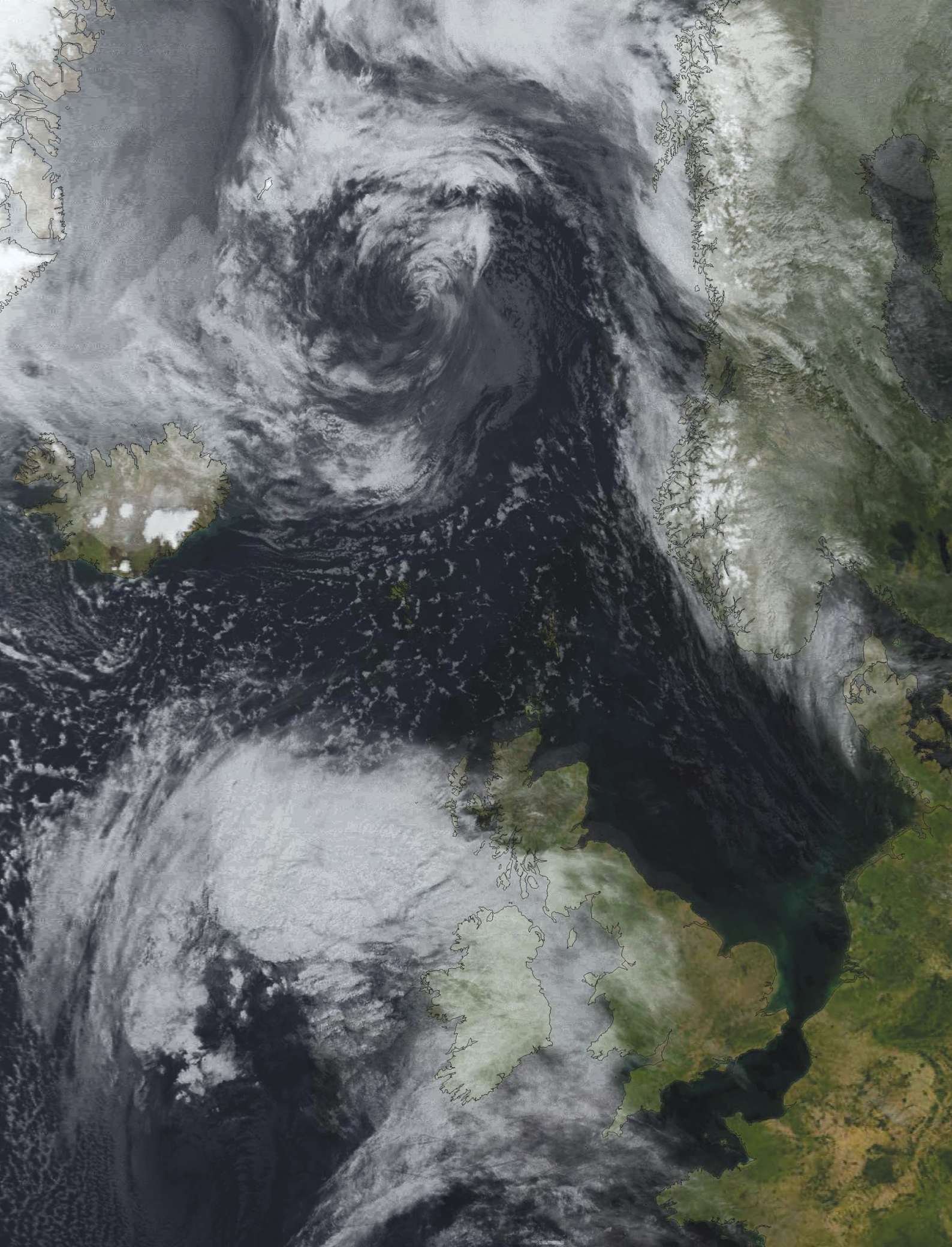
The Antarctic Peninsula, jutting out into the Southern Ocean from West Antarctica, is one of the fastest warming places on Earth. Most of its glaciers are receding. The uptick in new vegetation in recent years also coincides with a decrease in Antarctic sea-ice extent, an increase in open water, and a strong positive phase in the Southern Annular Mode, which could be producing warmer, wetter conditions, the authors noted.

<https://www.antarcticglaciers.org/glaciers-and-climate/southern-annular-mode/>

As plant life finds more favourable conditions for growth on the Antarctic Peninsula, questions about biodiversity in its unique habitats arise. 'The narrative in these places has been dominated by glacial retreat,' Roland said. 'We're starting to think about what comes next, after ice recession.' Of particular concern is that where there's moss, soil formation tends to follow, creating more opportunity for nonnative plants to find a foothold. When that happens, maintained Bartlett, 'you're looking at potentially an erosion of biodiversity.'

Antarctica hosts hundreds of native species of mosses, liverworts, lichens, and fungi, but only two native species of flowering plants. Human presence on the continent for tourism and research can result in the introduction of non-native species (although seeds and spores can also arrive on the wind). Several cases of invasion have already been documented in the northern Antarctic Peninsula and nearby islands. 'Biosecurity will become increasingly critical as temperature limitations on cold, high-latitude ecosystems decrease,' wrote the researchers.

Now, the scientists are keen to return to the field to understand the changes in finer detail. "We're at the point that we've said the best we can say with the Landsat archives," Roland said. Many questions remain as to what types of plant communities comprise these new green areas and what shifts in the structure and function of the Antarctic Peninsula's ecosystems may already be underway. 'We need to go to these places where we're seeing the most distinctive changes and see what's happening on the ground.'



Storm Darrah imaged on December 6, 2024 as it approached the British Isles, imaged at 15.26 UT by Meteor M2-4
MCIR Image: Joachim Scharrer

A23a Nears South Georgia Island

Copernicus Image of the Day

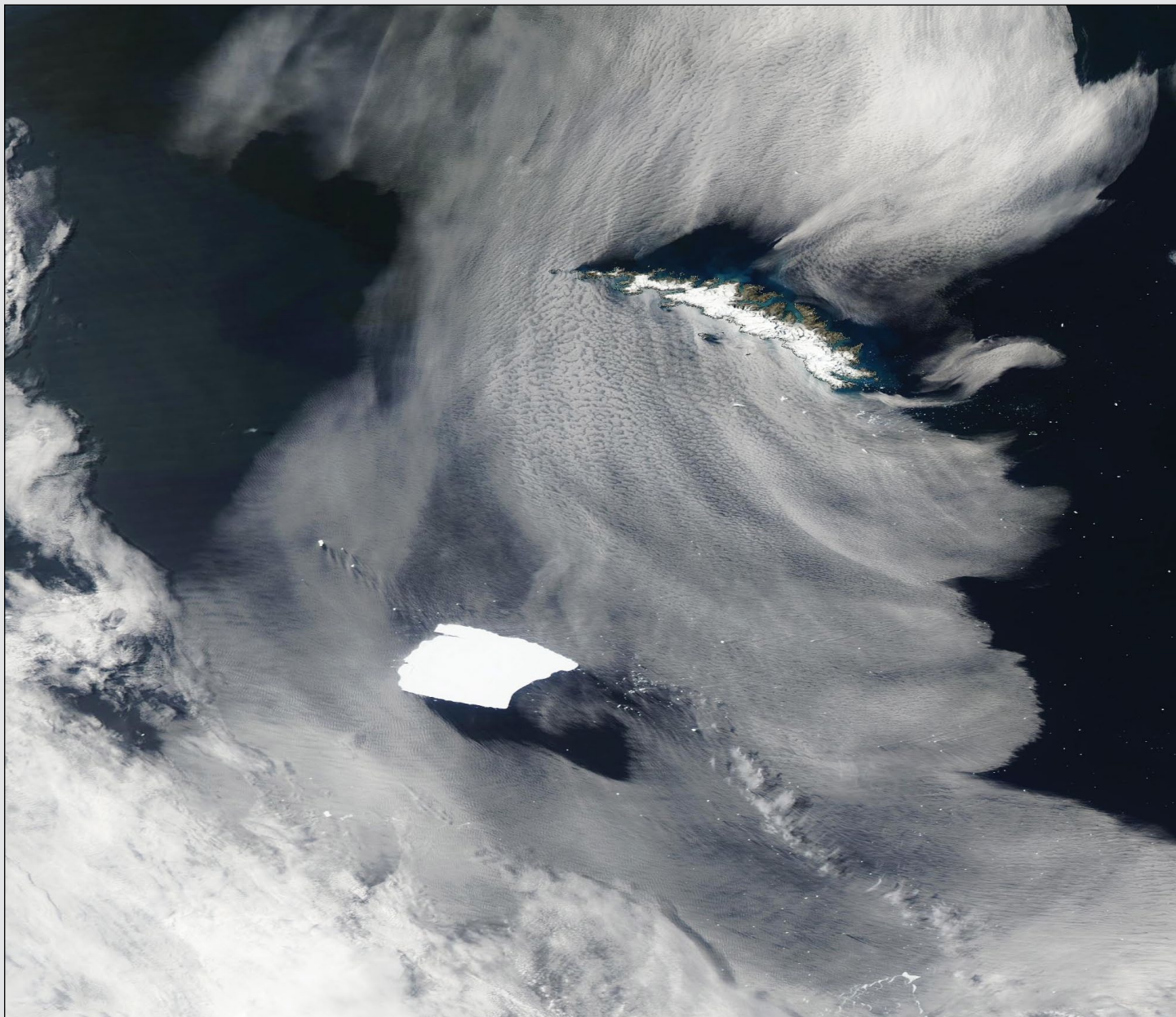


Image Credit: MODIS Land Rapid Response Team, NASA GSFC

On January 15, 2025, the Moderate Resolution Imaging Spectroradiometer (MODIS) on NASA's Aqua satellite captured the world's largest iceberg drifting towards South Georgia Island. In this image, the bright white rectangular-shaped Iceberg A23a floats roughly 250 kilometres off the southern tip of crescent-shaped South Georgia Island. Clouds swirl around both the island and the iceberg while brilliant streaks and swirls of blue and green colour the waters of the South Atlantic Ocean.

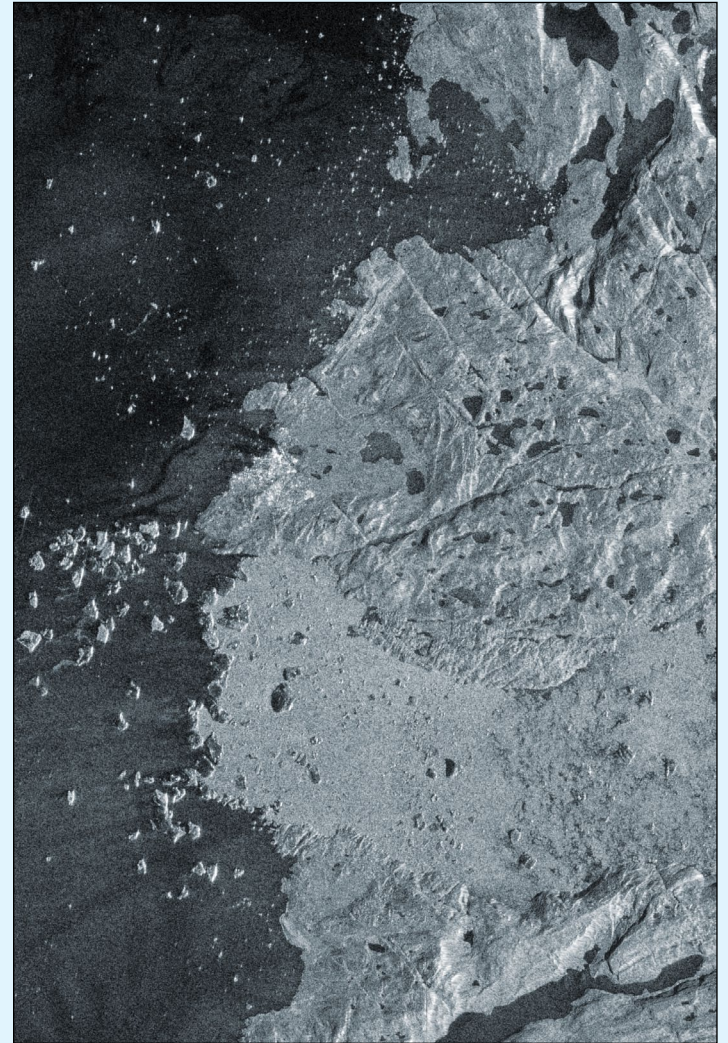
After breaking from the Filchner-Ronne Ice Shelf in 1986, Iceberg A23a spent decades stuck to the floor of the southern Weddell Sea. It began to wriggle loose in the early 2020s, and by March 2023 the Rhode Island-sized iceberg floated unencumbered. But such freedom lasted only a year. As it drifted northward during March 2024, the 'berg became ensnared by a rotating vortex

of water—or Taylor column—caused by currents encountering a bump on the sea floor. It continued to spin in that location until, after making 15 rotations, the 'berg broke out of the spin-cycle in November 2024. It has been drifting freely since, floating on currents that transport roughly 90 percent of icebergs from the Weddel Sea toward the South Atlantic Ocean.

Currents also shape the streaks of colour north of South Georgia Island. The blues and greens mark the location of a large phytoplankton bloom. These microscopic plant-like organisms thrive in the cold, nutrient-rich water near the southern tip of South America, which is located 2,157 kilometres west of South Georgia Island. Phytoplankton blooms float freely in the upper levels of the ocean, pushed and pulled by currents.

Jakobshavn Glacier, Greenland

European Space Agency



Images contain modified Copernicus Sentinel data (2024), processed by ESA
Licence: CC BY-SA 3.0 IGO or ESA Standard Licence

These summer images from the Copernicus Sentinel-2 and Sentinel-1 missions showcase different satellite views of Greenland's west coast. The optical Sentinel-2 image on the left, acquired on August 5, 2024, highlights the mouth of the Ilulissat Icefjord, clearly visible in white. This fjord is home to the Jakobshavn Glacier, known as Sermeq Kujalleq in Greenlandic, one of the fastest and most active glaciers in the world.

Jakobshavn Glacier drains approximately 6.5% of the Greenland ice sheet and produces around 10% of its icebergs. Many of these icebergs are so large that they become grounded in shallower areas of the fjord, where they remain for years until melting sufficiently to break apart and disperse. Several icebergs in the

image appear as white dots scattered across the fjord, speckling the waters of Disko Bay like stars in the night sky.

These towering icebergs, some reaching heights of 100 metres above the water, conceal even larger portions beneath the surface. Their shapes, sizes and colours vary greatly. Despite their appearance, some of the largest icebergs pictured here have a perimeter of two kilometres.

Just north of the fjord's mouth lies the small town of Ilulissat, with the town's airport visible in light brown further north. Ilulissat, which means 'icebergs' in Greenlandic, is a popular destination for tourists who come to see the giant icebergs passing near the port.

The radar image on the right, captured on August 3, 2024 by Copernicus Sentinel-1, shows the positions of the giant bergs two days prior to the Sentinel-2 acquisition.

By comparing these two images, the movement of the icebergs can be tracked. Their movement depends on various factors, including size, sea depth, currents and wind. In this region, icebergs typically drift northward towards Ilulissat.

Radar missions like Sentinel-1 are remarkably useful in monitoring sea ice, ice sheets and drifting icebergs, particularly in polar regions. Unlike optical imaging, radar can acquire images under any weather conditions, day or night.

Bloom off of Australia

MODIS Web Image of the day

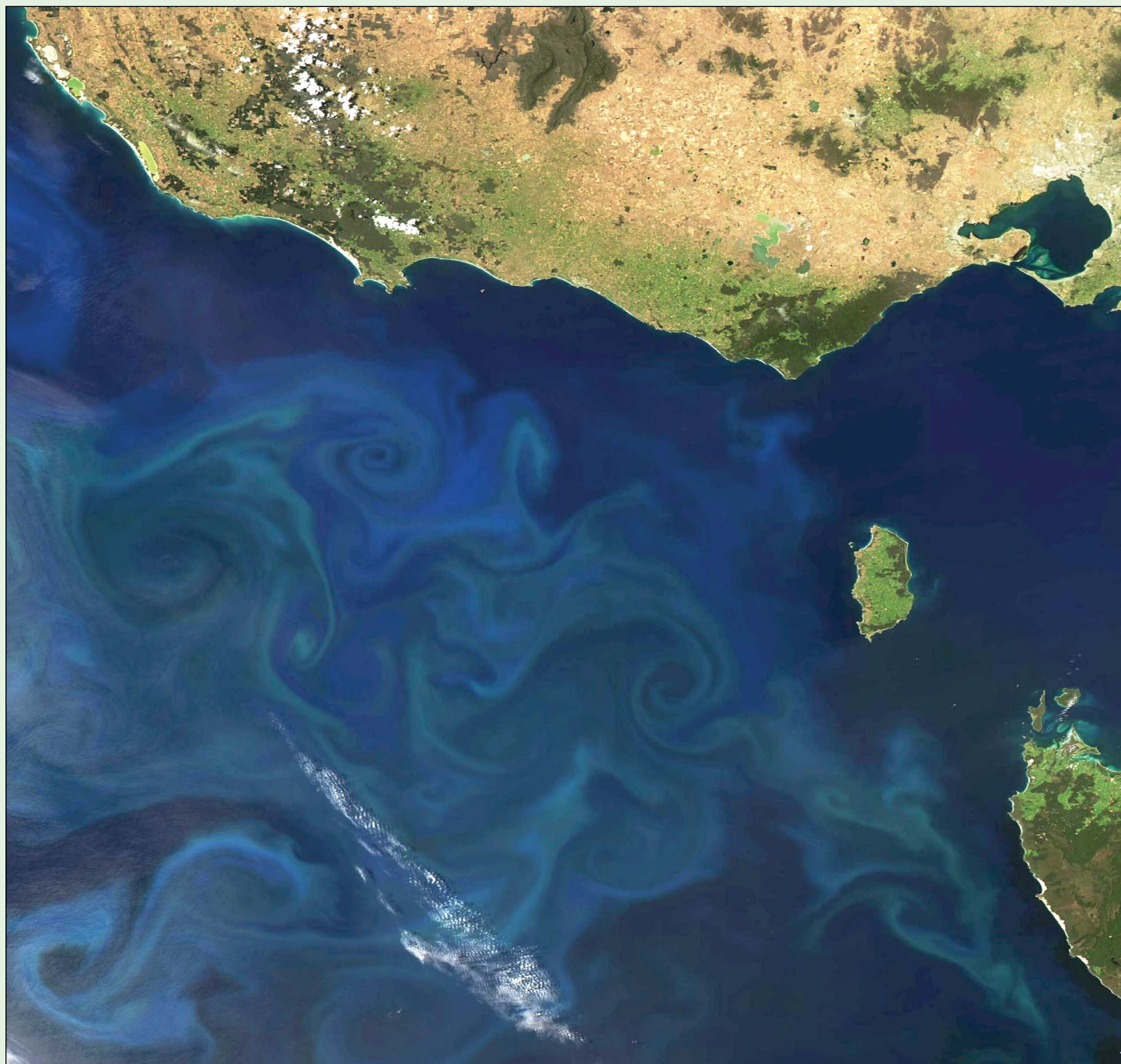


Image Credit: MODIS Land Rapid Response Team, NASA GSFC

Bright swirls of green and blue stretched across the Great Australian Bight for more than 800 kilometres in early December 2024. The Moderate Resolution Imaging Spectroradiometer (MODIS) on NASA's Aqua satellite acquired this true colour image of the intense colours on December 5.

The colours are the result of an enormous bloom of phytoplankton—microscopic plant-like organisms that carry chlorophyll and other pigments. Phytoplankton live in these waters year-round in relatively small numbers but, when they have adequate food, sunlight, water temperatures,

and oxygen content in the water, the tiny organisms can reproduce explosively to form massive floating blooms that can be seen from space. The swirls are created by the blooms being carried along by currents and eddies in the water.

Conditions in the Great Australian Bight become favourable for phytoplankton each austral summer. Seasonal winds, storms, and ocean currents tend to mix the water columns in this region, redistributing nutrients. In addition, water temperature rises and daylight length increases. All these factors are ideal for phytoplankton growth.



Enrico Gobbetti sent in this striking image from Russia's Elektro L3 geostationary satellite, operating from 165.8° east, that he acquired at 12.42 UT on December 3, 2024

Satellites Spot a 'Ghost' Island

NASA Earth Observatory

Story by Lindsey Doermann



NASA Earth Observatory images by Wanmei Liang, using Landsat data from the U.S. Geological Survey.

This image, divided into three panels, shows the same area of the Caspian Sea during November 2022 (left), February 2023 (centre) and December 2024. The left image shows featureless blue water but, at the top of the centre image, a small island has appeared with a tail of lighter-coloured water stretching down from it. The right-hand image shows a much smaller island and plume.

An island emerged from the Caspian Sea after a mud volcano erupted in early 2023. By the end of the following year, it had almost completely eroded away, retreating from view like an apparition. Powerful eruptions of the Kumani Bank mud volcano have produced similar transient islands several times since its first recorded eruption in 1861. Also known as Chigil-Deniz, the feature is located about 25 kilometres off the eastern coast of Azerbaijan.

The OLI (Operational Land Imager) and OLI-2 on the Landsat 8 and 9 satellites captured these images showing the island emerge and shrink. In

November 2022, the crest of the volcano remained below the sea surface. By February 14, 2023 (middle), an island had appeared with a sediment plume drifting away from it. Additional satellite observations suggested that the island emerged between January 30 and February 4 and measured approximately 400 metres across, according to University of Adelaide geologist Mark Tingay. By the end of 2024 (right), a greatly diminished portion of Kumani Bank was visible above the water.

Kumani Bank's previous eight recorded eruptions occurred in bursts lasting less than two days and produced islands of different sizes and life spans. A May 1861 event resulted in an island just 87 metres across rising 3.5 metres above the water: it eroded away by early 1862. The strongest eruption, in 1950, produced an island 700 metres (2,300 feet) across and six metres tall.

Mud volcanoes are '*weird and wonderful features that remain largely understudied and little understood,*' stated Tingay during a seminar for the Geological Society of Australia.



NASA Earth Observatory image by Wanmei Liang, using Landsat data from the U.S. Geological Survey.

Ranging in size from a couple of metres to several kilometres across, most mud volcanoes are found in areas with active tectonics or high sedimentation rates. These are places where subsurface pressure can build and force a mix of fluids, gases, and sediments to the surface.

And these features may not be unique to this planet: scientists think that some muddy mounds in the northern lowlands of Mars may have formed when gas- and liquid-rich sediments spewed out on to the surface.

The satellite image above shows a coastal area of Azerbaijan on the left and the dark blue Caspian Sea on the right. Coastal waters are cloudy with sediment, and the Kumani Bank mud volcano appears as a speck in the sea with a sediment plume streaming south from it.

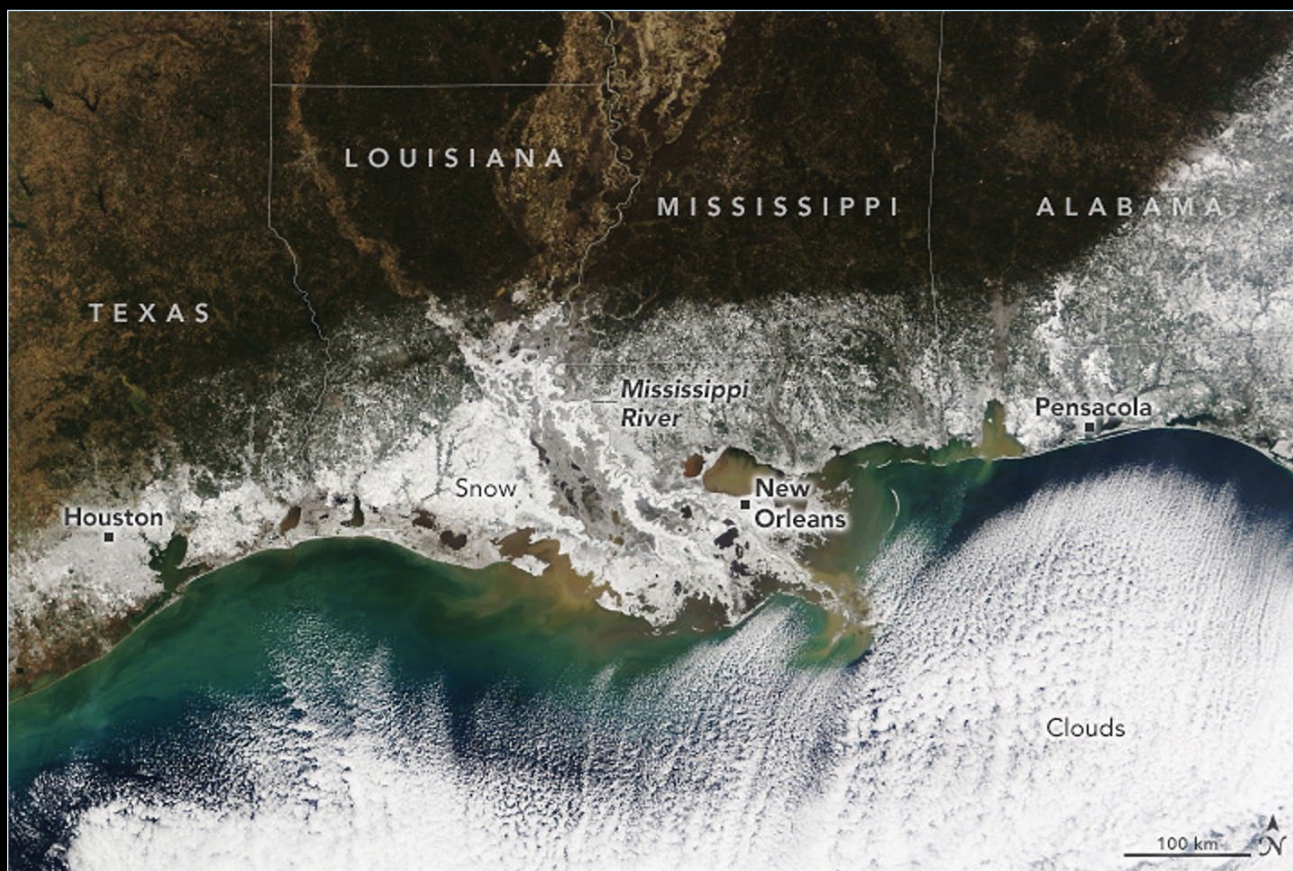
On Earth, Azerbaijan is unusual for its high concentration of mud volcanoes. Geologists have tallied more than 300 in eastern Azerbaijan and offshore in the Caspian Sea, with most of those occurring on land. The region falls within a convergence zone where the Arabian and Eurasian tectonic plates are colliding.

Mud volcano eruptions can be hazardous, with the potential to expel large amounts of material—and even flames—over a short period of time. Azerbaijan’s mud volcanoes are linked to the South Caspian Basin’s vast hydrocarbon system and are known to emit flammable gases such as methane along with the characteristic muddy slurries. It is uncertain if the 2023 Kumani Bank eruption was fiery, but past eruptions of this and other nearby mud volcanoes have sent towers of flame hundreds of metres into the air.

Southern States Frozen Over

NASA Earth Observatory

Story by Emily Cassidy



NASA Earth Observatory image by Wanmei Liang, using MODIS data from NASA EOSDIS LANCE and GIBS/Worldview

A satellite image of the USA Gulf Coast, centred on Louisiana, shows a swath of white snow coating southern parts of Louisiana, Texas, Alabama, and Florida. The snow looks especially bright along the winding course of the Mississippi River.

A winter storm brought below-freezing temperatures and heavy snow to the southeastern United States in January 2025. The storm dumped record snowfall on the region, prompting flight cancellations and the closure of more than 320 kilometres of Interstate 10, according to news reports.

Temperatures plunged into the single digits in southern Texas and Louisiana on January 22, when an arctic air mass met with a low-pressure system over the Gulf Coast. The airport in Baton Rouge recorded a temperature of -14°C , the lowest measured there in 95 years of record keeping.

Bands of winter weather brought blizzard conditions to southwestern Louisiana, a region unaccustomed to snow and ice. Wind gusts of 50 to 65 kilometres per hour accompanied the heavy snow and led to limited visibility. Several cities saw all-time records for snow totals on January 22, including New Orleans, Louisiana; Mobile, Alabama;

and Pensacola, Florida. About 20 centimetres of snow fell in New Orleans and 13 centimetres in Pensacola.

Flakes continued to fall in the Carolinas and southeast Virginia on January 22, when the MODIS (Moderate Resolution Imaging Spectroradiometer) on NASA's Terra satellite acquired this image. Large swaths of the Gulf Coast look like a frozen tundra. Bright white snow along the winding course of the Mississippi River stands out.

'Many of the old river channels of the Mississippi can be seen in the image,' stated Alex Kolker, a professor of coastal geology at the Louisiana Universities Marine Consortium. 'In a delta like this, riverbanks are higher than other areas because sediment was deposited here over many years. These lands accumulated a little more snow and show up brighter in the image.'

The rare storm brought more snow to New Orleans than has fallen in Anchorage, Alaska, since the start of this meteorological winter, noted the National Weather Service. Cold lingered in the south on the morning of January 23, and large stretches of Interstate 10 were still closed due to icy conditions.

Sado Island's Riches

NASA Earth Observatory

Story by Lindsey Doermann

Whether it conjures up the letter 'S', a lightning bolt, or perhaps an asymmetrical butterfly, the shape of Japan's Sado Island is somewhat peculiar. The tripartite geography features two parallel mountain ranges of volcanic origin, offset by an alluvial plain. In the hills, volcanic activity formed gold and silver deposits that people mined for centuries, while on the plains, traditional rice cultivation coexists with ecological conservation efforts.

The OLI (Operational Land Imager) on Landsat 8 acquired this image of Sado Island on April 22, 2024. Japan's sixth largest island, it lies approximately 35 kilometres off the west coast of Honshu, the country's main island. The volcanic activity that formed the rocks of Sado's mountains and its gold and silver deposits occurred around 20 million years ago.

During that period of volcanism, magma-heated water containing gold and silver rose toward the surface through cracks in the rock. The metals precipitated out in the fractures, forming the deposits that humans would later exploit.

Mining took different forms in the southern mountains compared with the north. In the south, erosional and tectonic processes left gold deposits in granular form, known as *placer gold*, on or near the surface. In the northern range, minerals remained locked in veins running deep into the mountains and sometimes exposed at the surface.

Panning for gold in the Nishimikawa Placer Gold Mine may have begun as early as the 12th century, while the Aikawa-Tsurushi Gold and Silver Mine, with its intricate network of tunnels, was developed in the late 1500s. The Sado mines were the leading producer of gold in the world for part of the Edo period (1603–1868), when approximately 40 tonnes of gold and 1,800 tonnes of silver were extracted. These sites, along with archaeological remains of the non-mechanised



NASA Earth Observatory image by Wanmei Liang, using Landsat data from the U.S. Geological Survey.

mining methods used there, comprise a 2024 addition to the list of UNESCO World Heritage sites.

In the lowlands, Lake Kamo is a large brackish water body known for its farmed oysters. Across the centre of the island, a network of rivers cuts through a patchwork of fields. People have cultivated rice on the plains of Sado for centuries, expanding into the hills and creating terraced paddies during the height of gold mining.

Over the past 15 years, Sado rice farmers have endeavoured to balance agriculture with biodiversity by nurturing feeding habitat for the endangered crested ibis (*Nipponia nippon*) in their paddies.

The wading birds became extinct in Japan in 2003, but according to news reports, reintroduction efforts and modified farming practices have resulted in ibis numbers exceeding 500 on Sado Island in 2022.

Ice on Lake Erie

MODIS Web Image of the Day



Image Credit: MODIS Land Rapid Response Team, NASA GSFC

Fiercely cold winds swept across the Great Lakes during January 2025, spurring a rapid growth of lake ice. Air temperatures in Toledo, Ohio and Erie, Pennsylvania plummeted from highs near 10°C in the closing days of December 2024 to well below freezing mid-month. On January 22, Erie experienced lows of -20.6°C and, at the other end of Lake Erie, thermometers registered -19.4°C in Toledo.

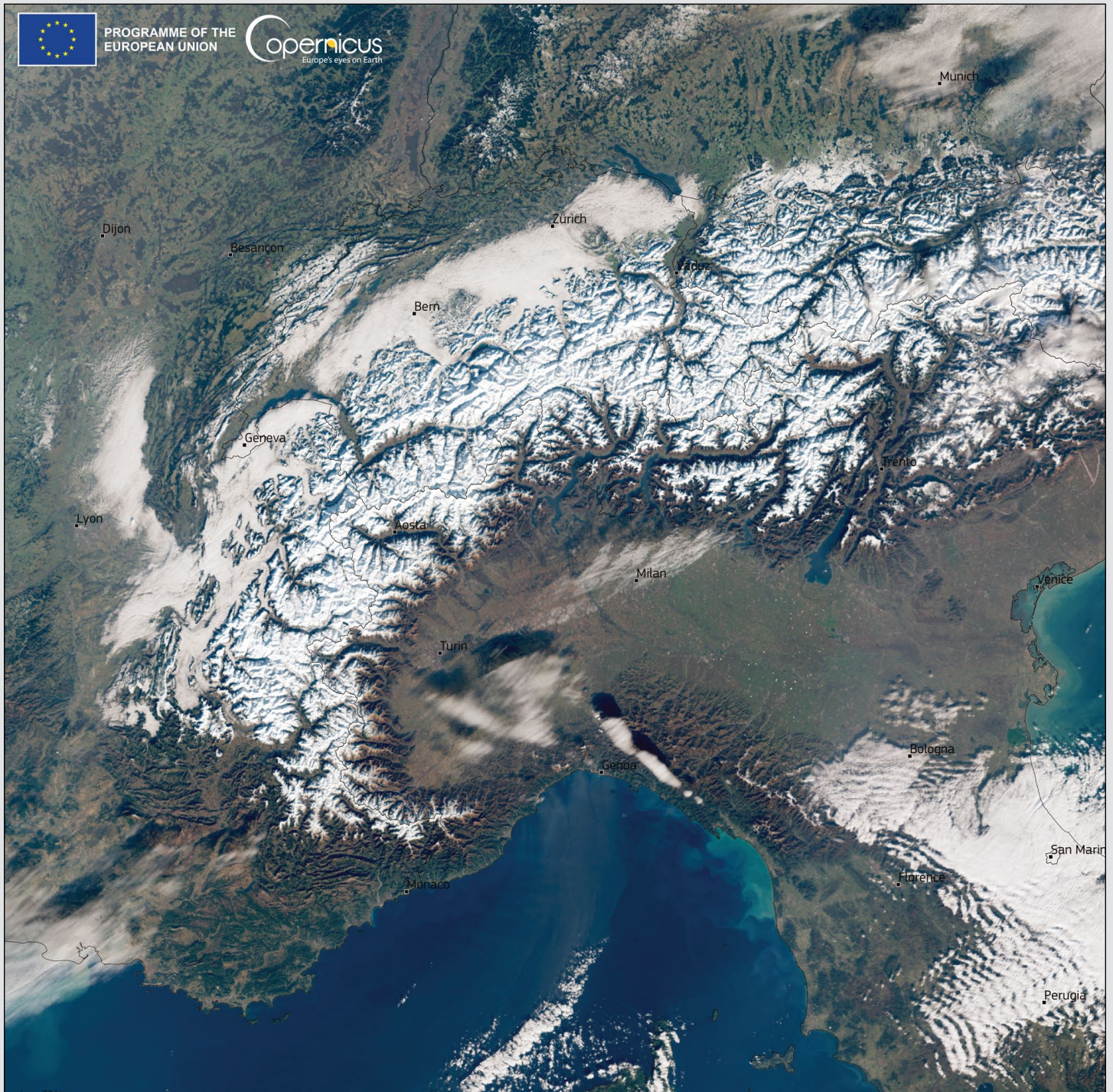
By January 25, Lake Erie responded to the deep Arctic blast by undergoing a rapid ice-up, with ice covering up to 86% of the lake, according to data from the *National Oceanic and Atmospheric Administration* (NOAA). This is well above average ice cover for this time of year, and above the annual peak average ice coverage, which typically occurs in mid-February.

The Moderate Resolution Imaging Spectroradiometer (MODIS) on NASA's Aqua satellite acquired this true-colour image of ice on Lake Erie on January 27. The far western section of the lake, near Toledo, was covered in fast ice (ice that sticks to the shoreline) as was a smaller section of ice on the eastern edge, near Erie.

By January 27, total ice cover had decreased from the January 25 peak due to a combination of warming air, sunshine and strong wind. Wind gusts of up to 93 kilometres per hour were reported at Niagara Falls, near the east side of the lake, with frequent gusts in the range 56-74 kilometres per hour measured on January 26-27. Strong winds push drifting ice, frequently causing it to pile up, resulting in increased open water.

Snowfall in the Alps in Line with Historical Averages

Copernicus Image of the Day



Credit: European Union, Copernicus Sentinel-3 imagery

This Copernicus Sentinel-3 image acquired on January 14, 2025 shows the Alps covered in snow.

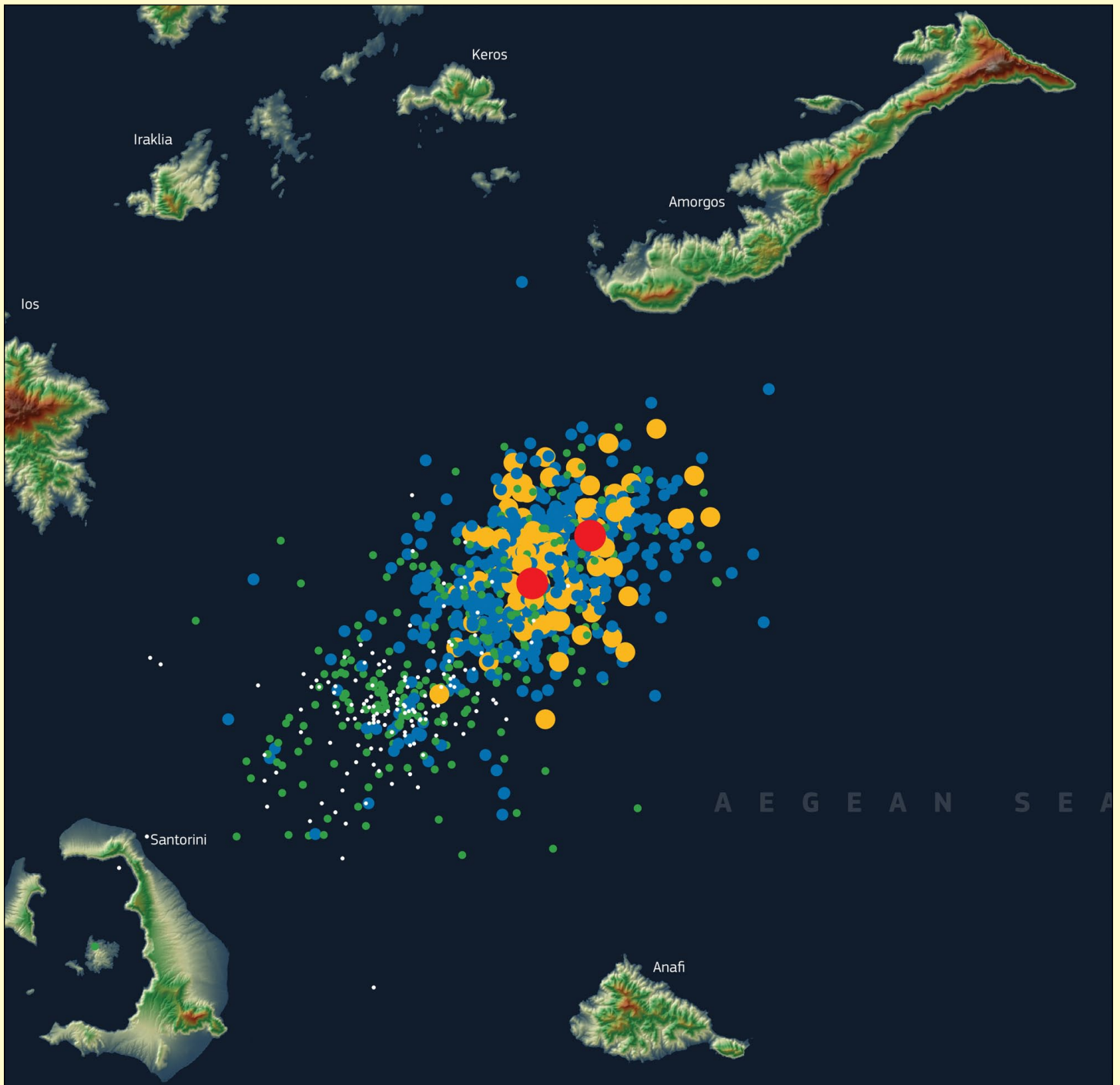
After a start to the season characterised by an absence of precipitation, the January 2025 cold wave which swept across much of Europe brought abundant snowfall to the Alps, transforming the mountain range into a snowy landscape ideal for winter sports enthusiasts. These cold temperatures favoured significant snow accumulations, which

reached levels in line with historical averages for this time of year.

In some areas, the accumulations were particularly abundant: in Switzerland, the snow pack in some areas measured 140 centimetres, while in Italy some peaks reached 240 centimetres. In France, up to 175 centimetres of snow were recorded in some areas while in Austria, the snowpack measured up to 120 centimetres.

Seismic Swarm in the Cyclades Islands, Greece

Copernicus Image of the Day



Credit: European Union, Copernicus Digital Elevation Model

Since January 27, 2025, the Cyclades Islands have been struck by more than 1,000 undersea earthquakes, with some exceeding a magnitude of 5.0. The earthquakes' epicentres have mainly been located between the islands of Santorini (lower left) and Amorgos (upper right).

The continuous tremors have prompted thousands to leave

Santorini. Approximately 6,000 people have departed using planes, boats, and private yachts. On February 3, emergency rescue crews were deployed, as authorities advised residents to drain swimming pools and avoid areas prone to rockfalls due to the island's steep cliffs.

This data visualisation, generated using data from the *Copernicus*

Digital Elevation Model, geo-localises the seismic swarm. It also includes indicators for the epicentres and magnitudes of the earthquakes which have occurred since the onset of the seismic crisis.

Copernicus data is useful for studying the consequences of seismic and volcanic activity, helping to support emergency operations around the globe.

Tropical Cyclone Zelia

MODIS Web Image of the day

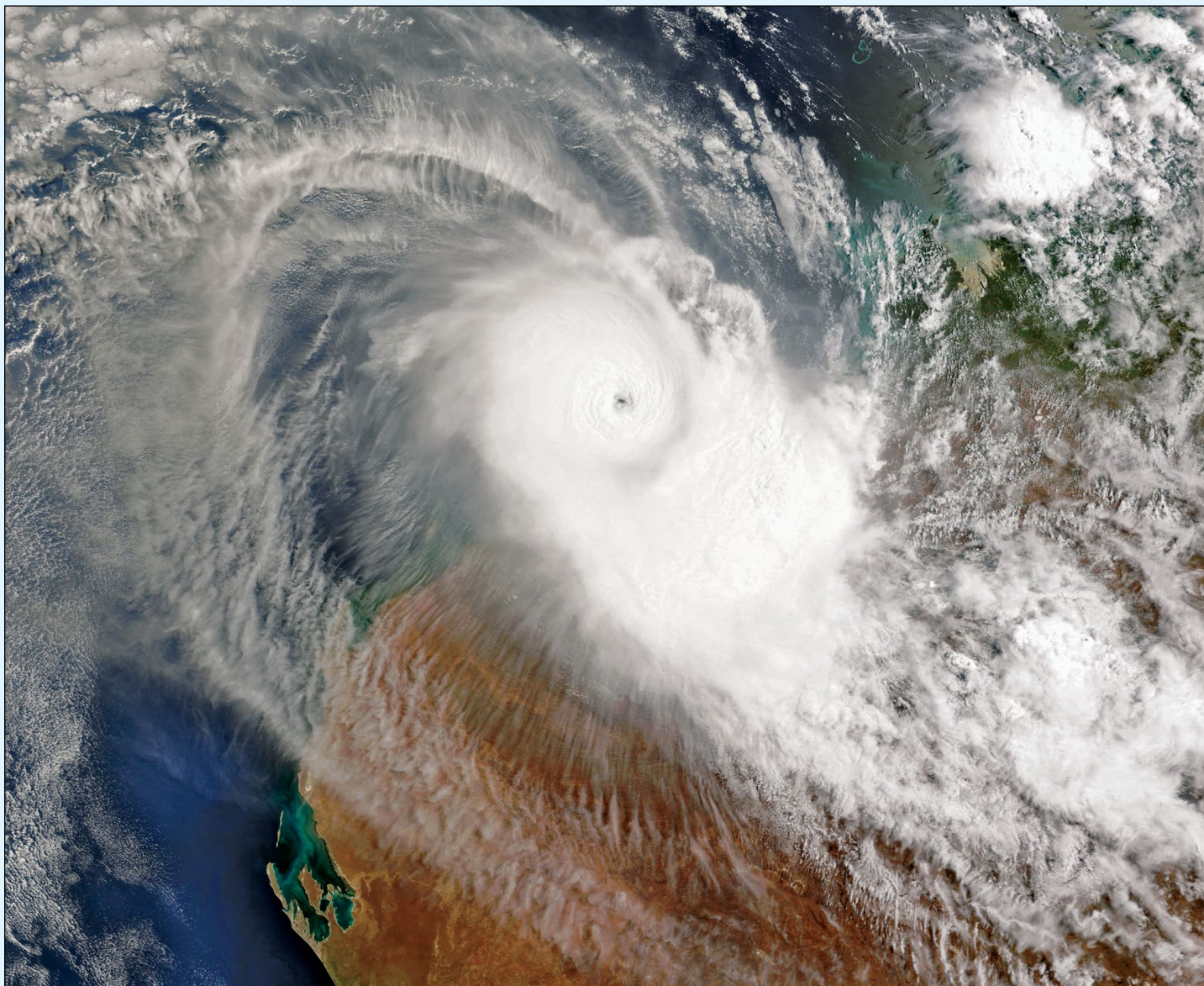


Image Credit: MODIS Land Rapid Response Team, NASA GSFC

Severe Tropical Cyclone Zelia was approaching landfall on February 13, 2025, when the Moderate Resolution Imaging Spectroradiometer (MODIS) on NASA's Terra satellite acquired this true-colour image. The fearsome and sprawling storm sported a large cloud-free eye as the southeast quadrant brought wind and rain to the state of Western Australia.

Near the time this image was acquired, Zelia was carrying maximum sustained winds of about 260 kilometres/hour), which is the equivalent of a strong Category 5 hurricane on the Saffir-Simpson Hurricane Wind Scale. ABCNews (Australian Broadcasting Company) reported that the storm was forecast to bring wind gusts of up to 320 kilometres per hour.

At 6.56 am AWST on February 14, the *Australian Bureau of Meteorology* (BoM) noted that Zelia was located about 90 kilometres north of Port Hedland and 220 kilometres north of Marble Bar. It was moving to

the south southeast and was expected to make landfall later in the day near or to the east of Port Hedland as a Category 5 storm.

At 7.15 am AWST on February 14, the *Department of Fire and Emergency Services WA* issued a Cyclone Emergency Warning advising those between Pardoo to Whim Creek and inland to west of Marble Bar to

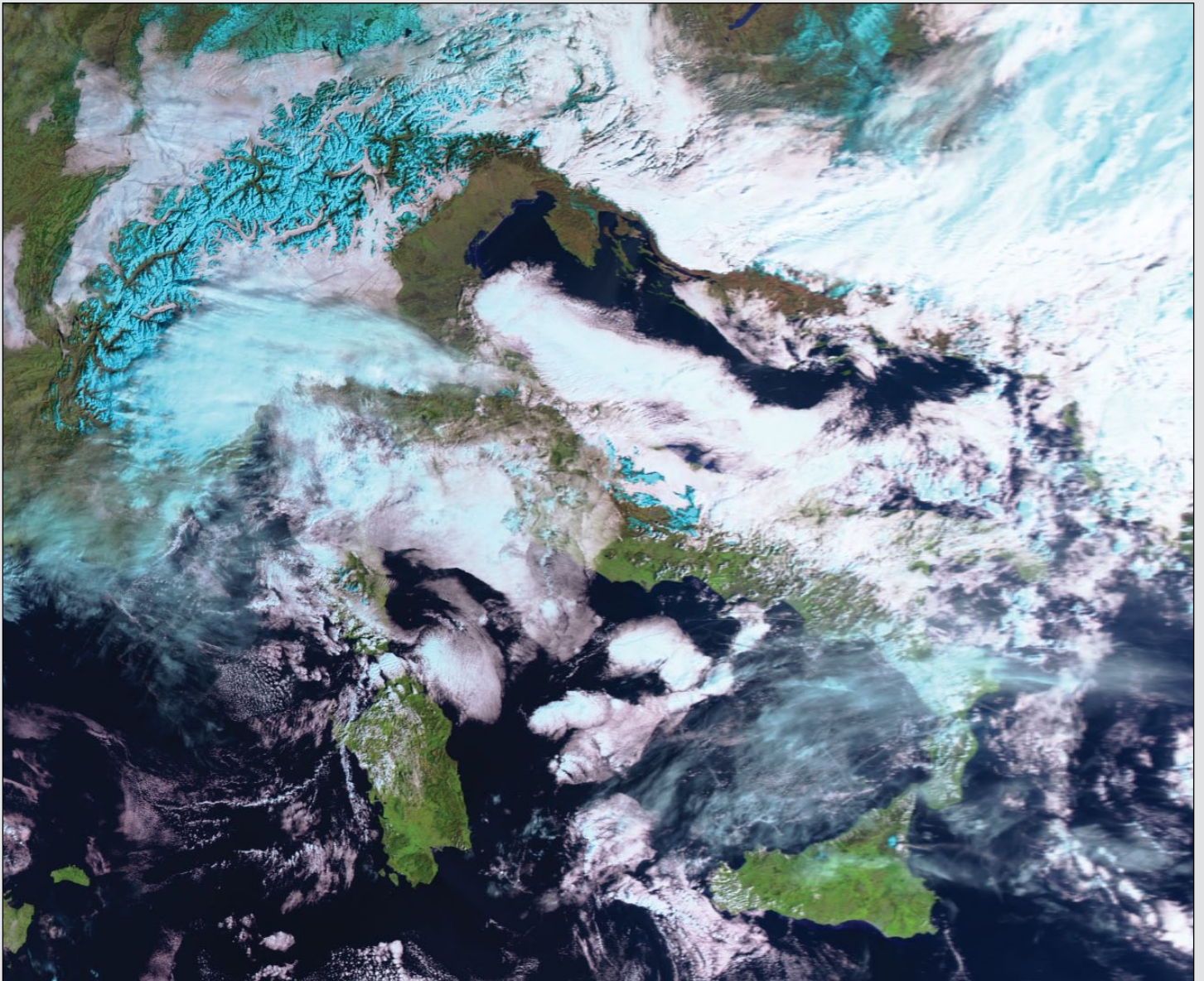
“SHELTER INDOORS NOW”

The advice noted that “it is too late to leave now”.

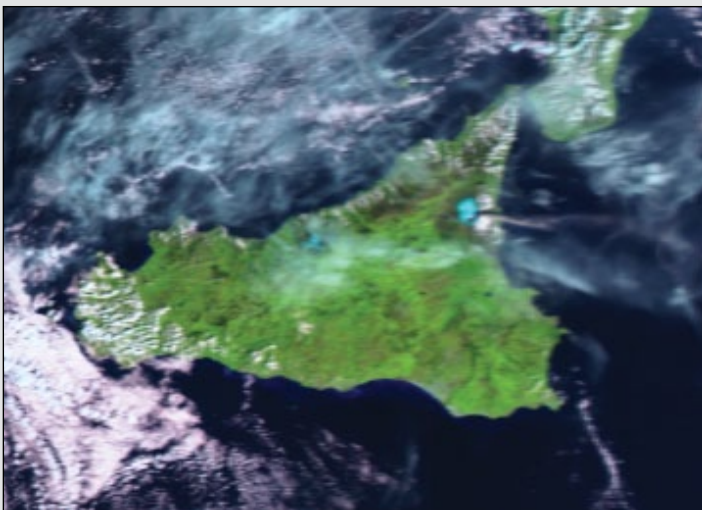
Additional advice to other locations, to prepare for the oncoming storm, was also published as well as advice on closing of roads, parks, and schools. Residents between Wallal Downs and Wickham including Port Hedland were specifically warned of an especially dangerous storm tide as the cyclone centre crosses the coast.

Etna Eruption

Enrico Gobbetti



The snow-covered Alps and Italy as viewed from Metop-C at 09.32 UT on February 17, 2025



This clip from the Metop C image shows the eruption plume from Etna more clearly.

On the right is a photograph of my new setup for receiving weather Satellite imagery.

I am also currently working to try to receive images in the X-Band



Central Italy

MODIS Web Image of the Day



Image Credit: MODIS Land Rapid Response Team, NASA GSFC

The sky was clear and bright over central Italy on November 23, 2024, allowing the Moderate Resolution Imaging Spectroradiometer (MODIS) on NASA's Aqua satellite to acquire this true-colour image of the region. Swirls of tan sediment colour the waters off the coasts of the long Italian peninsula, both in the Mediterranean Sea in the northeast and the Tyrrhenian Sea to the southwest. Italy has faced stormy weather, with heavy winds, rain, and flooding, in several locations since mid-November. The foul weather undoubtedly contributed to coastal run-off of sediment into the seas. In the south, snow caps the highest elevations of the Apennine Mountains, the long range that makes

up the spine of peninsular Italy. Also notable is a series of lakes that spot the southern peninsula in central Italy. These circular lakes have formed in calderas, depressions that form after violent, explosive eruptions empty a volcano's underlying magma chamber. Over time, the rims of a caldera can collapse into the interior, and the depression fills with water. The most notable caldera lake in the image is the turquoise-tinted Lake Trasimeno, located near the centre. The bright colours seen in these waters are a mix of sediment, which is easily stirred up by wind in the shallow lake, and a growth of tiny single-celled organisms known as phytoplankton.

Nested Calderas of Zavaritskogo Volcano

NASA Earth Observatory

Story by Lindsey Doermann

In the remote northwest corner of the Pacific Ocean, a dotted line of islands stretches between northern Japan and Russia's Kamchatka Peninsula. The Kuril Archipelago is sparsely populated by humans but riddled with volcanoes. Simushir Island, in the centre of the archipelago, contains four volcanoes, two of which bear craters partly filled with water (figure 1).

The Zavaritskogo volcano is a striking feature on Simushir. It is made up of nested, steep-walled calderas surrounding a central lake. The OLI (Operational Land Imager) on Landsat 8 captured these images of Zavaritskogo on September 12, 2024.

The youngest caldera, centred in figure 2, is partially outlined by reddish, unvegetated slopes. Since its formation, small eruptions starting around the year 1910 produced cinder cones and lava domes within its bounds. The last documented volcanic activity, in 1957, spewed material that filled in the northwest part of the lake, including a dome 350 metres wide and 40 metres tall. The satellite image shows a detailed view of the Zavaritskogo caldera, composed of concentric circular depressions. Most of the land is green with vegetation. The innermost depression is ringed partly by reddish rock and contains a lake and a lava dome.

Past eruptions, however, were much more powerful. New research suggests that Zavaritskogo's inner caldera may have formed in one of the planet's largest volcanic eruptions during the 19th century.

Previous analyses of polar ice cores indicated that a major eruption in 1831 had injected several metric tons of sulphur into the stratosphere, reflecting solar radiation back to space and causing the Northern Hemisphere to cool by up to 1° C. And historical accounts from that summer note that the Sun appeared green, purple, and blue, which may occur



Figure 1 - Simushir Island showing its four volcanoes



Figure 2 - The caldera of Zavaritskogo volcano
NASA Earth Observatory images by Wanmei Liang, using Landsat data from the U.S. Geological Survey

when volcanic particles in the atmosphere scatter sunlight. The probable volcanic source of these phenomena, however, had long remained elusive.

Scientists have now matched the chemical composition of volcanic material—preserved in ice cores—with that from the most recent major eruption of Zavaritskogo. Radiocarbon dating and estimates for the

volume of material ejected from the volcano further implicated Zavaritskogo as the source of the major 1831 eruption.

More volcanic mysteries from that era are left to be solved, the study's authors noted. The sources of two other eruptions in the early 19th century, signified by sulphur spikes in ice core data, have yet to be identified.

Currently Active Satellites and Frequencies

Polar APT / LRPT Satellites				
Satellite	Frequency	Status	Format	Image Quality
NOAA 15	137.6200 MHz	On	APT	Intermittent sync problem
NOAA 18	137.9125 MHz	On	APT	Good
NOAA 19	137.1000 MHz	On	APT	Good
Meteor M N2	137.1000 MHz	Off	LRPT	Failed
Meteor M N2-3	137.9000 MHz	On	LRPT	Variable ^[1]
Meteor M N2-4	137.9000 MHz	On	LRPT	Good

Polar HRPT/AHRPT Satellites				
Satellite	Frequency	Mode	Format	Image Quality
NOAA 15	1702.5 MHz	Omni	HRPT	sync problem
NOAA 18	1707.0 MHz	RHCP	HRPT	Good
NOAA 19	1698.0 MHz	RHCP	HRPT	Good
Feng Yun 3C	1701.4 MHz	RHCP	AHRPT	Inactive ^[2]
Feng Yun 3D	7820.0 MHz	RHCP	AHRPT	Active ^[2]
Feng Yun 3E	7860.0 Mz	RHCP	AHRPT	Commissioning
Metop B	1701.3 MHz	RHCP	AHRPT	Good
Metop C	1701.3 MHz	RHCP	AHRPT	Good
Meteor M N2-2	1700.0 MHz	RHCP	AHRPT	Active ^[8]
Meteor M N2-3	1700.0 MHz	RHCP	AHRPT	Active
Meteor M N 2-4	1700.00 MHz	RHCP	AHRPT	Active

Geostationary Satellites				
Satellite	Transmission Mode(s)		Position	Status
Meteosat 9	HRIT (digital)		45.5°E	IODC - On
Meteosat 10	HRIT (digital)	LRIT (digital)	0°	On ^[4]
Meteosat 11	HRIT (digital)	HRIT (digital)	9.5°E	On ^[3]
Meteosat 12	HRIT (digital)	HRIT (digital)	0.4°W	On
GOES-13	GVAR 1685.7 MHz	LRIT 1691.0 MHz	61.6°E	^[5]
GOES-14	GVAR 1685.7 MHz	LRIT 1691.0 MHz	105°W	Standby
GOES-15 (W)	GVAR 1685.7 MHz	LRIT 1691.0 MHz	135°W	Off (in storage)
GOES-16 (E)	GRB 1686.6 MHz	HRIT 1694.1 MHz	75.2°W	On ^[7]
GOES-17	GRB 1686.6 MHz	HRIT 1694.1 MHz	104.7°W	Off
GOES 18	GRB 1686.6 MHz	HRIT 1694.1 MHz	137.0°W	On ^[7]
Himawari-8	No direct download	Data is only available via the HimawariCast service	140.7°E	On
Himawari-9	No direct download		140.7°E	On
Feng Yun 2E	SVISSR (digital)	LRIT (digital)	86.5°E	Off
Feng Yun 2F	SVISSR (digital)	LRIT (digital)	112.5°E	Standby
Feng Yun 2G	SVISSR (digital)	LRIT (digital)	105.0°E	On
Feng Yun 2H	SVISSR (digital)	LRIT (digital)	79.0°E	On
Feng Yun 4A	HRIT (digital)	LRIT (digital)	99.5°E	On
Feng Yun 4B	HRIT (digital)	LRIT (digital)	105°E	On

Notes

- 1 Currently, M2-3 and M2-4 transmit on 137.9 MHz but have on occasions switched to 137.1 MHz. Transmission is currently on a Symbol Rate of 72,000 baud, though 80,000 baud has been used in trials.
- 2 These satellites employ a non-standard AHRPT format and cannot be received with conventional receiving equipment.
- 3 Meteosat prime Full Earth Scan (FES) satellite
- 4 Meteosat prime Rapid Scanning Service (RSS) satellite.
- 5 Repurposed for use by the US Space Force
- 6 GOES 15 also transmits EMWIN on 1692.700 MHz GOES 16 also transmits EMWIN on 1694.100 MHz GOES 17 also transmits EMWIN
- 7 GOES Rebroadcast (GRB) provides the primary relay of full resolution, calibrated, near-real-time direct broadcast space relay of Level 1b data from each instrument and Level 2 data from the Geostationary Lightning Mapper (GLM). GRB replaces the GOES VARIable (GVAR) service.
- 8 Following a collision with a micrometeorite, the power system aboard Meteor M2-2 has been compromised. AHRPT is still being transmitted when the solar panels are sunlit, but there is insufficient battery power to enable the LRPT stream.
- 9 Japanese satellites MTSAT-1R (Himawari-6) and MTSAT-2 (Himawari-7) are no longer active and are probably retired. Current Japanese operational geostationary satellites are Himawari-8 and Himawari-9.